Optical studies of functionalized graphene and similar 2D materials

Submitted by James Nicholas Milton to the University of Exeter as a thesis for the degree of
Doctor of Philosophy in Physics
in September 2017

Abstract

In this thesis, the functionalization of few layer graphene is examined and measured using Raman spectroscopy and two probe electrical measurement, with the goal of obtaining graphene shapes on a nanometre scale which retain the properties lent to them by a functionalization process. Graphene is a material of great interest currently since the properties of single and few layer graphene are unique due to its layered structure and electronic band dispersion. The functionalization in this case serves to increase carrier concentration and thus the conductivity of graphene, which is thin, light, transparent and flexible. Thus technologies such as flat or curved screen TVs, computers, and wearable devices are exploring many avenues to improve such devices. Graphene, and functionalized graphene, may be one way to achieve enhancements or replace components in these emerging technologies.

In addition to graphene, similar two dimensional materials (TaS_2 and $NbSe_2$) were also measured using Raman spectroscopy, with the goal of both measuring the Raman spectra of the materials and observing the effect of progressively exposing the samples to the incident Raman laser light. The possibility of using the Raman laser to remove layers from these materials is briefly examined as a way of obtaining few or single layer samples for further studies.

The main result given in this thesis is that few layer graphene nanoribbons can be created with widths of 500nm and thinner, which can retain Iron Chloride between the layers to affect increase the conductivity of the ribbon. Another result noted was for an experiment with few layer graphene and plasmon grids, where the intensity of scattered light decreased as the number of graphene layers increased, without a shift in the spectral position of the resonance peak. Finally, in examining TaS_2 and $NbSe_2$, the preliminary tests seem to show that it is possible to etch both these materials using the laser from a Raman spectrometer, and thus control the thickness of these materials in a controlled way.

The material samples in this thesis as well as the measurements carried out on them and the analysis of the data gathered afterwards were almost entirely carried out by myself. Though the exception is chapter 5, the measurement of plasmons, which was done in equal collaboration with fellow PhD student Dmitry Polyushkin.

Contents

List of Figures

Chapter 1

Introduction

1.1 2D materials

The majority of the time, solid materials are found, used and tested in bulk three dimensional forms with many well tested and predictable properties. Some layered materials can be reduced to either a two dimensional single layer or a few layered system. These usually have different and interesting properties and characteristics from the majority of bulk materials. Many are far less studied than their bulk forms due to the added difficulties of producing and measuring a thin layer of it.

There are three types of common two dimensional materials[16]. The first is a layered van der Waals solid, which has strong in-plane covalent bonding and weak out of the plane van der Waals or hydrogen bonding. These materials can be easily mechanically or by liquid, exfoliated to a thinner number of layers. Layered ionic solids is a second class of two dimensional materials which consists of a charged polyhedral layer sandwiched between hydroxide or halide layers by electrostatic forces. Exfoliation can be achieved using ion intercalation or ion exchange liquid exfoliation methods. Finally there are surface assisted nonlayered solids which are artificially synthesized on a surface using chemical vapour deposition or epitaxial growth.

2D materials allow for the study of certain properties in a unique way, such as taking the application of Hooke's law to an extreme case − two dimensions. Normally in a 3D material the atoms are too randomly orientated and arranged in the bulk to investigate the specific constants in a given direction. In a 2D layer the stress responds very differently for in plane and out of plane stresses and shears, which enables precise measurements of the constants.

1.1.1 Graphene

One of the most studied and reported on 2D materials at the moment is graphene, which is a single layer of carbon atoms, with a hexagonal lattice structure (figure 1.1). It was first discovered in 2004 by Giem and Novoselov[17] using the mechanical exfoliation process, also known as the scotch tape method. It was thought before graphene was discovered that two-dimensional materials would not be stable due to thermal instabilities forcing them to assume a 3D form[18]. This may be the case if the graphene was suspended in mid air, but while lying on a silicon substrate or suspended between two contact points, graphene remains very stable.

There are many different possible applications thought of for graphene in the future. It is stronger and stiffer than diamond, is a very good conductor of heat and electricity and is impermeable to liquids and gases[3]. The majority of applications

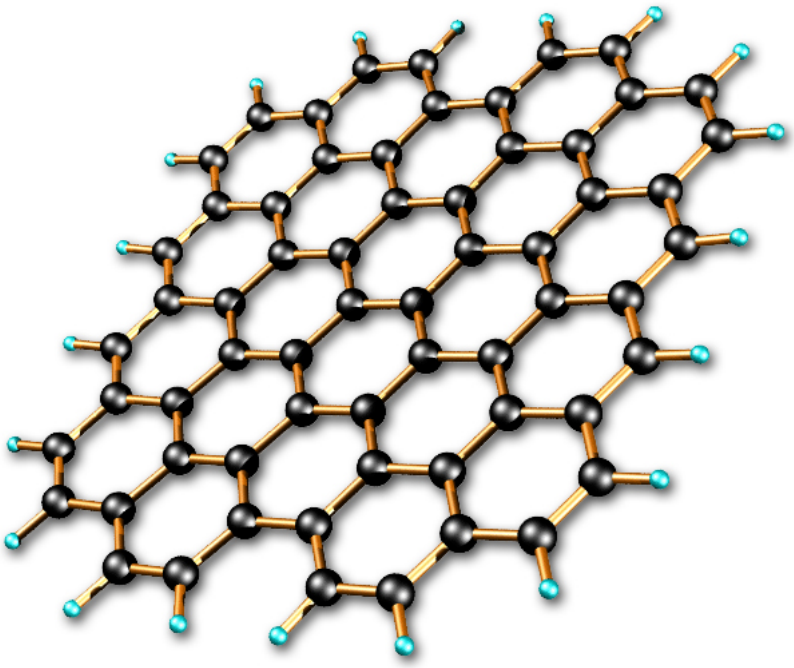

Figure 1.1: The hexagonal two dimensional structure of graphene. *Copyright: Chris Ewels (http://www.ewels.info).*

surround computer electronics with some speculation that it could be a common material to include in many different electronic systems. One problem for some applications to overcome is graphene's gapless electronic spectrum preventing the conduction being turned off, though there are some ways to modify the system to solve this problem. Another application is a use in transmission electron microscopy (TEM) as a supporting crystal membrane. Another use is as a part of individual ultra high frequency analogue transistors, usually based on GaAs, used in many communication technologies. Graphene could extend these devices functionality to operate in the terahertz frequency range, using ballistic transport of charges which graphene is capable of. Graphene powder can be used as a filler for composite materials as well as possibly improving super capacitors, batteries, interconnects, and field emitters. In optoelectronic applications a graphene based coating could be applied or printed to improve many products such as solar cells and liquid crystal displays, competing with indium tin oxide (ITO), the current industry standard. The resistivity is higher than ITO but the transparency is greater at around 80%. If the resistivity can be improved then it is likely graphene could replace ITO for some applications. It does offer some advantages compared with ITO, such as being chemically stable, robust and flexible (including being folded). This adds the possibilities of more bendable and flexible technology in the future. It can be used as a base material in nanoelectromechanical systems (NEMS) for sensing purposes, making use of its lightness and stiffness.

Charge carriers in graphene layers can be changed in type or concentration using adsorbates or substrates[19]. p-type doping is caused by a difference between graphene's work function and the electron affinity of the adsorbate. This difference is at its simplest due to the gap between the highest occupied molecular level and the lowest unoccupied molecular level of the adsorbate and graphene. This can also be affected by the substrate as well, which is even more significant given the thinness

of graphene structures.

Two properties of graphene which could be improved for some applications are the lack of a band gap and the quantity of charge carriers for conduction. Opening a band gap can be achieved by changing the hybridization of the graphene electronic orbitals from sp2 to sp3; either by chemically bonding a molecule, or adding a functional group containing oxygen, or adding an element like fluorine or hydrogen, to the carbon structure of graphene.

1.1.2 Transition metal dichalcogenides (TMDs)

There are other 2D materials similar to graphene like the transition metal dichalcogenides (TMDs)(e.g. MoS_2, WSe_2, ZrS_2, $MoSe_2$, $NbSe_2$ and TaS_2), which consist of a layer of metal atoms arranged hexagonally between two layers of chalcogens, usually written in the form MX_2 (M=metal, X=chalcogen). For all these layered systems there is strong covalent bonding within the hexagonal layers and weak van der Waals interaction between the layers.

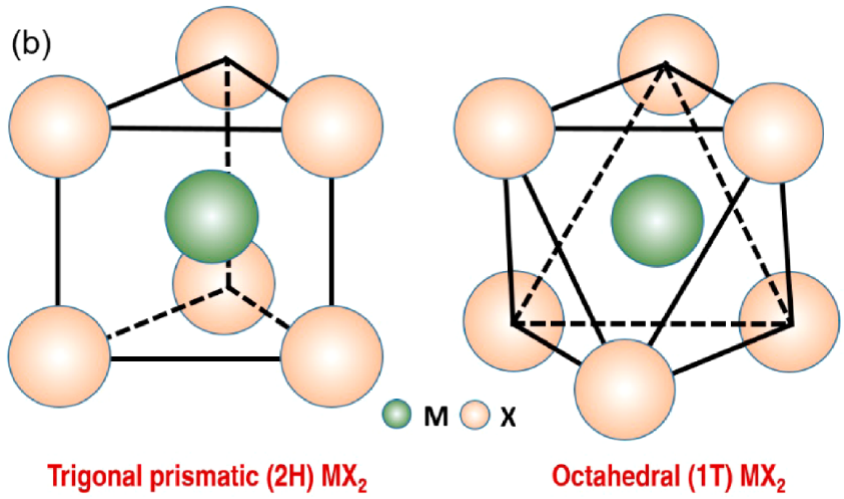

Figure 1.2: Unit cell structures for transition metal dichalcogenides[1]

Of the TMDs MoS_2 has probably received most research due to its interesting potential applications. WSe_2 has main applications for photovoltaic devices like solar energy collectors, due to a very high absorption coefficient for visible and infrared light.

Electronically TMDs have many different properties with HfS_2, GaS, and GaSe being insulators; MoS_2 and WS_2 being semi-conductors; and $NbSe_2$ and TaS_2 being metals. Most TMDs can also reach a super conducting state at very low temperatures (less than 7K). Intercalation of alkali metals or organic molecules into these layered structures can change semi conductors into metallic conductors or super conductors, and change metallic conductors into semi conductors.

Many of the properties of these layered materials are affected by their thickness, especially when there is only a single or few layers. Also the quality of the layer surface, amount of defects in the structure, and presence of other chemicals and molecules nearby or attached to the surface all can have an effect on the properties too. The most common way of achieving higher quality samples for study is by using tape to mechanically cleave the layers apart [20].

Several methods can be applied to characterize these layered systems, like scanning probe microscopy (SPM), scanning electron microscopy (SEM), transmission electron microscopy (TEM), optical microscopy, and Raman spectroscopy.

1.2 Summary of this thesis

This thesis focuses on the study of three materials in their two dimensional forms - graphene, TaS_2 and $NbSe_2$.

Chapter 2 gives a description of all three materials, giving background on their structures, their Raman spectra (which will be important given that a large part of the measurements were obtained from Raman studies) and some general and specific properties that are of interest for their study. Additionally, for graphene there is a description of different methods for functionalising it. Finally there is a description of plasmons for a two dimensional system, which will be applied to graphene.

Chapter 3 is a description of the methods for constructing the samples that were analysed (obtaining few layers, intercalation and patterning into measurable devices) and the methods for obtaining results (Raman and dark field study).

Chapter 4 is a report on the patterning of graphene into nanoribbon shapes with the addition of ferric chloride molecules as an intercalant. The amount and stability of the added molecules is measured using Raman spectroscopy and the conductivity is measured and compared with non intercalated systems measured by other groups.

Chapter 5 is a report on the use of graphene as a substrate to enhance the response of plasmons generated from a grid. Both non intercalated graphene and intercalated graphene is measured using dark field microscopy and Raman spectroscopy and compared with the signal when no graphene is present.

Chapter 6 is a report on TaS_2 as a few layer system, with measurements of the normal Raman spectrum as well as the spectrum after laser etching to reduce the number of layers further.

Chapter 7 is a report on $NbSe_2$ as a few layer system, with measurements of the normal Raman spectrum as well as the spectrum after laser etching to reduce the number of layers further.

Chapter 2

Background theory

Graphene is a two dimensional layer of carbon atoms arranged in a hexagonal lattice. As a single layer, it presents many unique properties which make it of interest for novel and new technology applications and solid state research, as well as quantum effects. This is due to the crystal structure allowing the electrons flowing through to act as massless Dirac fermions. This produces many effects which can not be studied in other systems.

2.1 Graphene properties

2.1.1 Band structure

The tight binding model can be used to calculate the band structure of graphene. If we start with a general case where there are series of equal atoms centred in the lattice positions $t_n = na$. We can consider a given local orbital Phi_a of energy E(k)

$$E_0 = \langle \phi_a(x - t_n)|H|\phi_a(x - t_n)\rangle \tag{2.1}$$

$$\gamma = \langle \phi_a(x - t_n)|H|\phi_a(x - t_{n\pm1})\rangle \tag{2.2}$$

γ represents the energy of the nearest atom. Consider γ as negative simulating s-like orbitals and attractive atomic potential

Now we use a Bloch sum to give us linear combinations of atomic orbitals (LCAO method):

$$\Phi(k, x) = \frac{1}{\sqrt{N}} \sum_n e^{ikt_n} \phi_a(x - t_n) \tag{2.3}$$

This satisfies Bloch's theorem as follows:

$$\begin{aligned} \Phi(k, x + t_m) &= \frac{1}{\sqrt{N}} \sum_n e^{ikt_n} \phi_a(x + t_m - t_n) \\ &= e^{ikt_m} \frac{1}{\sqrt{N}} \sum_n e^{ikt_n - t_m} \phi_a(x - t_n + t_m) \\ &= e^{ikt_m} \Phi(k, x) \end{aligned} \tag{2.4}$$

The energy dispersion is given by

$$E(k) = \langle \Phi(k,x)|H|\Phi(k,x)\rangle \tag{2.5}$$

$$E(k) = E_0 + 2\gamma \cos ka \tag{2.6}$$

$$E(k) \approx E_0 + 2\gamma - \gamma a^2 k^2 \tag{2.7}$$

$$m^* = \frac{\hbar}{2|\gamma|a^2} \tag{2.8}$$

When we apply this tight binding model in the specific case of graphene, we can start with describing the nearest neighbour atoms 1 and 2 with the following lattice vectors:

$$a_1 = -\frac{\sqrt{3}}{2}a_0 i + \frac{3}{2}a_0 j \tag{2.9}$$

$$a_2 = \frac{\sqrt{3}}{2}a_0 i + \frac{3}{2}a_0 j \tag{2.10}$$

We consider only the electrons in the 2pz orbitals of graphene. Bloch functions corresponding to the sublattices of carbon atoms 1 and 2 would then be as follows:

$$\chi_1 = \frac{1}{\sqrt{N}} \sum_n e^{i\mathbf{k}\cdot\mathbf{R}_{1n}} \varphi_1(\mathbf{r} - \mathbf{R}_{1n}) \tag{2.11}$$

$$\chi_2 = \frac{1}{\sqrt{N}} \sum_n e^{i\mathbf{k}\cdot\mathbf{R}_{2n}} \varphi_2(\mathbf{r} - \mathbf{R}_{2n}) \tag{2.12}$$

Let H be the Hamiltonian for an electron in the atomic potential given by the atoms in the graphene lattice. In order to calculate the terms

$$\langle \chi_i|H|\chi_i\rangle$$

. In the tight-binding formalism, only the following terms are considered:

$\langle \chi_a|H|\chi_a\rangle = \alpha$

$\langle \chi_a|H|\chi_b\rangle = \beta$

$\langle \chi_a\chi_b\rangle = \delta_{ab}$

Graphene has some unique properties due its structure, the main one being that it has a linear band structure. In a normal semiconductor the energy-momentum relation consists of a parabolic conduction band and valence band separated by a gap. What makes graphene special is that close to the Fermi energy (the energy of the highest filled electron state at absolute zero) its dispersion relation is linear and has no bandgap. This means that the speed of electrons is constant and independent of momentum, the same relationship as light which also has a constant speed c. So instead of the normal Schrödinger equation to describe the energy of an electron, the relativistic dispersion relation is a better starting place.

$$E^2 = p^2c^2 + m^{*2}c^4 \tag{2.13}$$

which in the limit of $pc << E$, becomes the much more famous equation of mass and energy equivalence $E = mc^2$.

With E the overall energy of the particle, p the momentum and c the speed of light. m^* is the effective mass of the electron, which as well as the normal electron mass, takes into account the effect of the periodic lattice on the electron. In a conventional semiconductor this would be related to the curvature of the parabolic energy-momentum relation.

$$\frac{1}{m^*} = \frac{1}{\hbar}\frac{\partial E}{\partial k} \tag{2.14}$$

This definition of effective mass is changed in graphene due to the hexagonal lattice structure. In graphene the lattice is chiral, which means it has areas in its structure which are mirror images and therefore are not super-imposable. Graphene has two triangular basis lattices which combine to form its hexagonal structure, and the effect on the electron is to cancel out its effective mass, making it equal to zero.

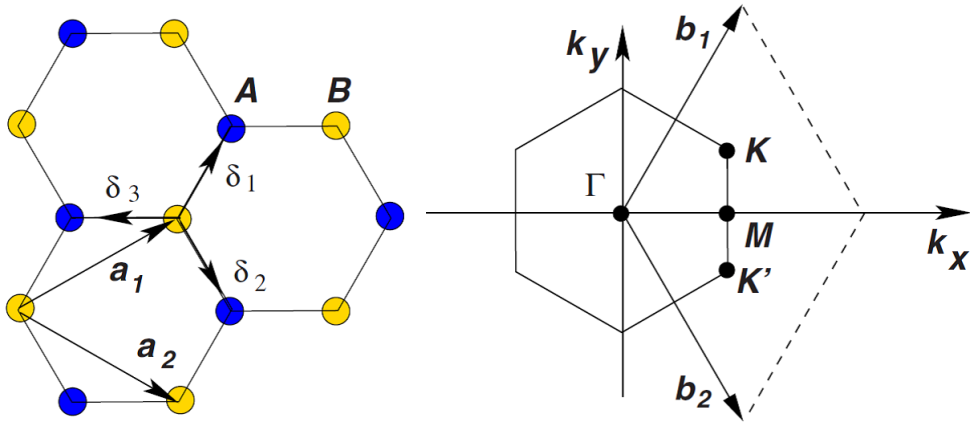

Figure 2.1: a) Diagram showing the separate sub-lattices of graphene A&B, b) the reciprocal lattice in k-space showing the Brillouin zone centres K and K′ [2]

The Dirac equation can be modified to account for this, and speed of light replaced by the Fermi velocity v_F (measured to be around $10^6 \mathrm{ms}^{-1}$[21]). The momentum has to become more complex as there are two lattices which provide the electrons with momentum in different directions. The Hamiltonian for the electron quasi-particles becomes more complex.

$$\hat{H} = v_F \vec{\sigma} \cdot \hat{p} \tag{2.15}$$

$$\hat{H} = \hbar v_F \vec{\sigma} \cdot \vec{k} \tag{2.16}$$

$$\hat{H} = \hbar v_f \begin{pmatrix} 0 & k_x - ik_y \\ k_x + ik_y & 0 \end{pmatrix} \tag{2.17}$$

$$\therefore E \propto \pm k \tag{2.18}$$

This is the low energy band dispersion for monolayer graphene calculated using the tight binding model using the first approximation (only hopping between nearest neighbours). This leads to two points per Brillouin zone (K&K′) and the Hamiltonian for each of these is shown here.

$$H_K = \hbar v_f \begin{pmatrix} 0 & k_x - ik_y \\ k_x + ik_y & 0 \end{pmatrix} \tag{2.19}$$

$$H_{K'} = -\hbar v_f \begin{pmatrix} 0 & k_x + ik_y \\ k_x - ik_y & 0 \end{pmatrix} \tag{2.20}$$

The dispersion for this at low energy is linear $E_k = \pm\hbar v_f \mid k \mid$. Monolayer graphene has a linear dispersion relation at low energy, which means electrons and holes act as massless Dirac fermions. Graphene has a very similar dispersion to light, which is the reason that electron optical effects and quantum phenomena can be seen in graphene. This behaviour means some interesting effects can be seen and studied in graphene, such as the unconventional integer quantum Hall effect, Klein tunnelling and Veselago lensing[22].

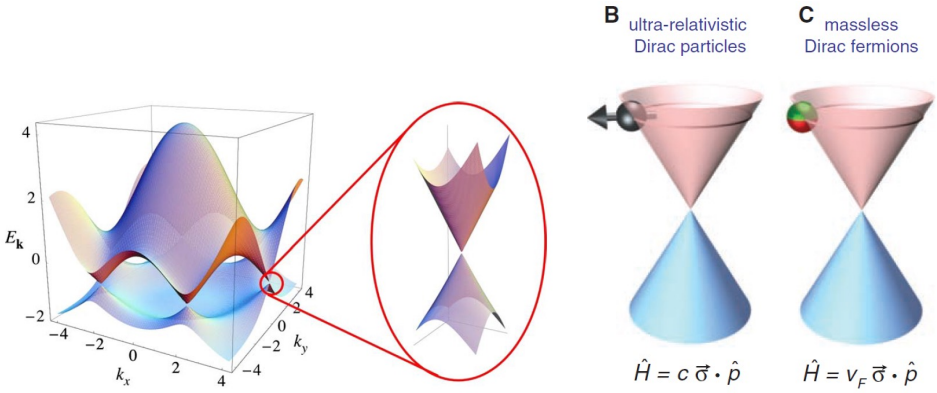

Figure 2.2: The electronic dispersion for the honeycomb lattice of graphene with a zoom on the low energy regime[2] and a comparison of the dispersion relation for light and that of graphene[3]

Monolayer graphene is not the only system with interesting properties, and multilayers of graphene have shown some very different and interesting properties so far in what is becoming a family of few layer graphene (FLG) materials. There are two known forms of crystal structure arrangements in FLG called ABA (AB, hexagonal, or Bernal) and ABC (rhombohedral) with different stacking manners.

The band structure of single layer graphene (SLG) is modified when more layers are placed on top. For band structures in Bernal-stacked FLG up to 5 layers it can be seen that the structure is no longer linear and adds many more subtle effects for future studies. So far bilayer and trilayer have been examined and it was found that Bernal stacked bilayer and rhombohedral-stacked trilayer exhibit a gate-tuneable bandgap while Bernal-stacked trilayer has a gate-tuneable overlap between conduction and valence bands.

The charge carriers in these multi-layered systems do have some effective mass but retain the chirality given to them by the sub-lattices of the graphene layers. These different band configurations are of great interest because these are the only materials where the gate can tune and control a gap or overlap between the conduction and valence bands.

2.1.2 Graphene properties

There are several properties of graphene which make its electronic structure a unique and interesting material to study. The first is the loss of effective mass for electrons

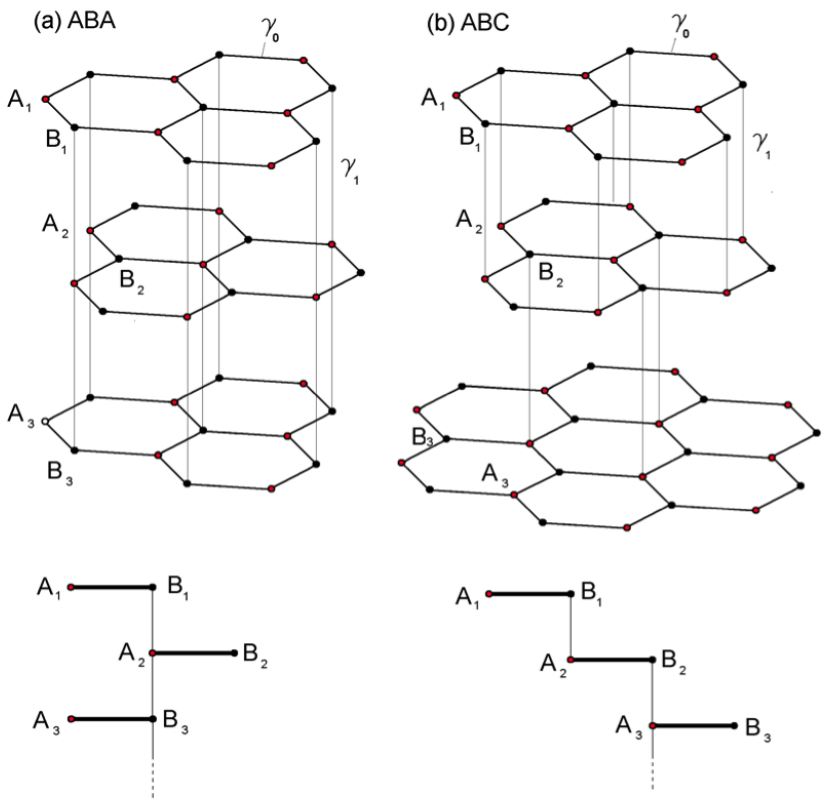

Figure 2.3: Atomic structures of multilayer graphenes with (a) Bernal-stacking and (b) rhombohedral stacking[4]

travelling through the two dimensional lattice, where they become Dirac like quasi-particles. This is a different system than most conducting materials described by the Schrödinger equation. Secondly, electrons moving through a graphene layer are much more accessible to scanning processes as well as being more sensitive to other materials close by. Thirdly, the quality of the electronic system is usually very high with electrons able to cover large distances without scattering (sub-micrometer scale). Fourthly, the quantum effects in graphene can be measured even at room temperature thanks to the massless electrons and low scattering.

The opacity of graphene is defined only by the fine structure constant, $\alpha = e^2/\hbar c \approx 1/137$ (where c is the speed of light), which is the parameter that describes the coupling of light to relativistic electrons. For a single layer of graphene the absorption of light has been found to be $\pi\alpha = 2.3\%$. The opacity increases by an additional 2.3% for each layer of graphene added, with a negligible reflectance and the opacity being independent of the wavelength of light[6]. This property favours the model where the high frequency dynamic conductivity G is a universal constant of $e^2/4\hbar$ for graphene.

Physically graphene has a breaking strength of 40 N/m, thermal conductivity of 5,000 $\mathrm{Wm^{-1}K^{-1}}$ at room temperature and a Young's modulus of 1TPa. It can be elastically stretched by up to 20%, which is more than any other crystal structure. Unusually graphene shrinks with any increase in temperature at any temperature, due to membrane phonons dominating in the two dimensional system. Graphene has high pliability (pleating and folding are common) as well as brittleness at high strain. It is impermeable to gases, including helium. It is currently unknown how

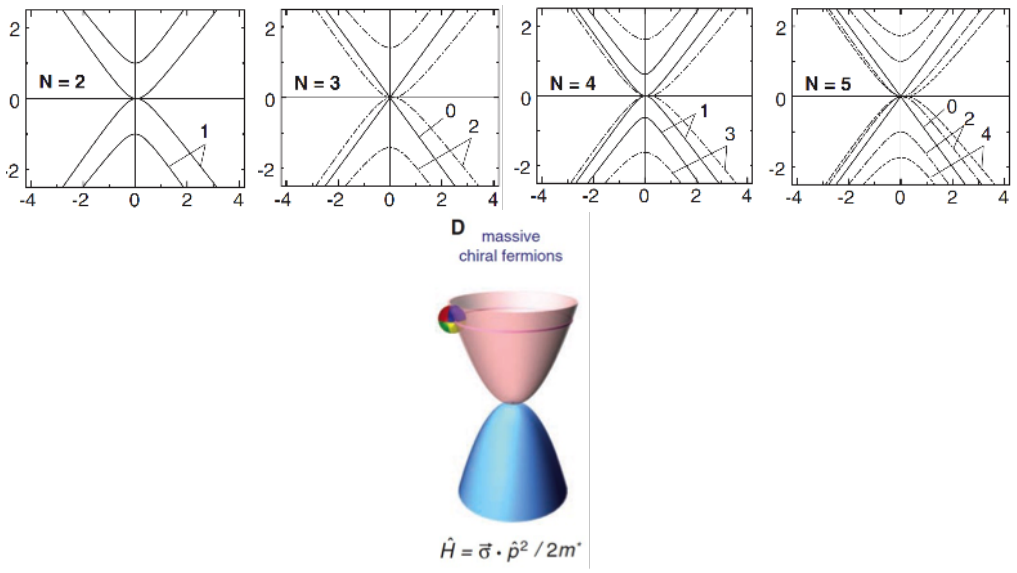

Figure 2.4: a) Band structures for multilayers of graphene for 2-5 layers[5] with the x-axis being $k_x/(\gamma/\gamma_1)$ and the y-axis being ε/γ_1 b) The modified low energy dispersion for bilayer[3]

it melts, including the melting temperature and the order of the phase transition.

2.1.3 Different ways to functionalize graphene

Intercalation is a method of inserting additional atoms or molecules of a different chemical species in between layers of a material in order to change the electrical, thermal or magnetic properties of that material. The number of free charge carriers can be varied extensively using this method. Many different reagents can be intercalated into graphene split into donor and acceptor types. Donors are mainly alkali metals (K, Rb, Cs, Li), alkaline earth metals or combinations of them with other compounds.

Acceptor intercalants are usually based around the halogens (Br_2, F_2, Cl_2), often in compounds with metals, as well as some acidic oxides and Brönsted acids. Most apart from $FeCl_3$ and $SbCl_5$ are unstable in air and require encapsulating to hold stability. Intercalation can be achieved using solids, liquids or gases as intercalants though vapour transport is the most common form for intercalation.

As a layered system, graphene can be functionalised in many different ways[23], and this section discusses some of them.

Graphene oxide can be formed by covalently bonding a functional group containing oxygen to the carbon atoms in the graphene. Once formed graphene oxide can contain several different functional groups such as carboxyl, hydroxyl, and epoxy groups. The oxygen can be removed later by other methods to produce reduced graphene oxide. It is thought that the epoxy and hydroxyl groups are present above and below the graphene layer, while carboxylic groups form on the edges of the graphene layer. Since the functional groups can be somewhat randomly attached to the graphene atoms, they give graphene oxide a more disordered and amorphous structure. It can be produced by either wet chemistry or plasma oxidation methods. Wet chemistry involves strong acids, which oxidize graphite and is then thinned by a liquid exfoliation process. Wet techniques are an advantage for large scale production but can produce contamination during the process. Another method

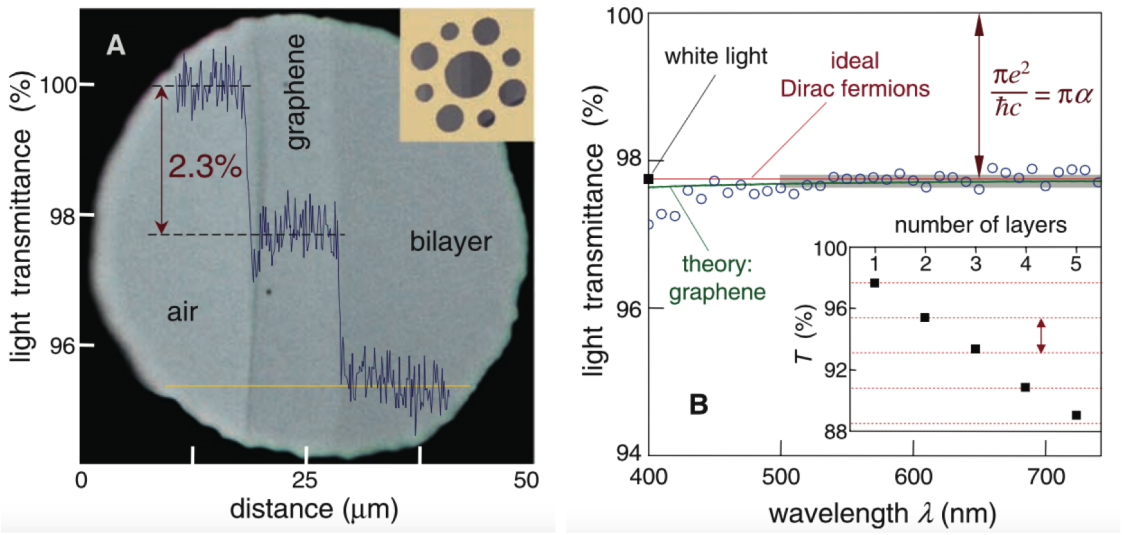

Figure 2.5: a) The intensity of transmitted light along the yellow line, going from air, to a single layer then a bilayer of graphene. b) The transmittance spectrum of single-layer graphene (open circles). The red line is the transmittance expected for two-dimensional Dirac fermions, whereas the green curve takes into account a nonlinearity and triangular warping of graphene's electronic spectrum. (Inset) The transmittance of white light as a function of the number of graphene layers (squares).[6]

of producing graphene oxide is the exposure of few layer graphene to a low power oxygen plasma. This can change the electronic properties of the graphene layers from a semi-metallic to a semiconducting behaviour. More control can be gained by using a water vapour plasma instead or by placing the samples to be oxidized downstream from the source of the plasma ions.

Other chemical elements can also be covalently bonded to graphene, such as hydrogen (forming hydrogenated graphene also called graphane), and fluorine (which forms fluorinated graphene also called fluorographene). This adsorbtion of chemical elements is called chemisorption and changes graphene hybridization from sp2 to sp3. In contrast to the oxidization of the graphene layers, hydrogenation or fluorination attaches the elements to the graphene layers in a very ordered way.

Hydrogenation can be achieved using several different methods including remote hydrogen plasma, an atomic hydrogen beam, electron induced dissociation of hydrogen silsesquioxane or Birch reduction.

Functionalizing with hydrogen opens a large energy gap, up to 3.5 eV for fully hydrogenated graphene. It also adds a large spin orbit interaction and possible magnetic properties, all originating from the change from sp2 to sp3 hybridization of the electronic orbitals.

Fluorination also changes the electronic orbitals from sp2 to sp3 and opens a band gap (up to 3.1eV) in the energy dispersion[23]. It is more stable than hydrogenated graphene, thanks to a stronger binding energy between fluorine and carbon atoms. Techniques for making it include a reaction between graphite and fluorine gas at around 400-600°C, exposure to fluorine based plasma, exposure to XeF_2, and laser irradiation of a fluoropolymer.

One advantage of functionalization using elements like fluorine and hydrogen is that there are ways to selectively choose which areas on the graphene surface are functionalized, which allows printing of circuits or patterns to make devices. This

can either be done by reducing areas from a fully functionalized graphene sheet or by functionalising specific regions of a pristine graphene layer.

Intercalation is another functionalization of few layer graphene by the introduction of molecules and/or atoms between the graphene layers without chemically bonding to the graphene structure. It can also separate the graphene from some substrate effects which are more coupled to the graphene layers in graphene grown by chemical vapour deposition (CVD) or epitaxial growth. The intercalation can modify the properties of graphene in a wide variety of ways depending on the substrate and the intercalant used. Examples include cobalt intercalated graphene on a substrate of Ir (111), where the functionalization has applications in spintronics; the intercalation of methane, which can open a controllable band gap; and the intercalation of bilayer graphene with Li on a SiC substrate, which may be useful in a nanoscale Li-ion battery and possibly open up a super conducting state. Graphene deposited on SiO_2, Si_3N_4, glass, or in liquid suspension has very little influence from the substrate and can be seen as quasi-free. Intercalation of few layer graphene on these substrates, with various elements and molecules opens up even more possibilities.

For bilayer graphene intercalants such as Br/Br_2 can result in a large charge transfer, enhancing the electrical conductivity; C,N or O can open a band gap (and with C and N atoms also possibly adding magnetic properties); Ni is predicted to make a non magnetic semi conductor with a moderate band gap; Fe and Co results in a ferromagnetic metallic system; and K may produce intrinsic superconductivity.

Experimentally K, Rb, ICl, IBr and $FeCl_3$ have been successfully intercalated into few layer graphene using vapour transport methods to place molecules in between the layers. The intercalated forms of few layer graphene produced commonly had an upshift in the Raman G peak showing the charge transfer either to or from the graphene, depending on whether the intercalant is a donor or acceptor. The resistance perpendicular to the graphene layers also increases due to a strong localisation of the high electronic orbitals.

Lithium can also be intercalated using graphene oxide; where the graphene oxide is first reduced chemically and filtered through a membrane and with the presence of lithium in the mixture becomes partially intercalated with lithium ions.

Finally graphene can be functionalised with the addition of colloidal quantum dots, which can increase the frequency dependant absorption of graphene. An effective band gap for graphene can also be added and tuned by varying the size of the quantum dots deposited on the graphene. The quantum dots have already been used as photoactive layers in other materials for light emission, photovoltaics, and photodetection. In graphene, the combination with quantum dots has enabled infrared and ultraviolet graphene photo detectors, using the quantum dots to generate charges, which then transfer to the graphene and are extracted through the drain electrode.

$FeCl_3$ in particular has shown an improvement in conduction for graphene while keeping it transparent. This is a prime candidate for a transparent conductor for use in displays, photovoltaics and wearable electronics.

2.1.4 Raman spectrum of graphene

Raman spectroscopy is the study of the response of a material when laser excitations of electrons in that material are modified by phonons (lattice vibrations). When a laser excites an electron from the valance band to the conduction band and the

electron relaxes back to the valance band, the photon emitted should be of the same wavelength because the energy given by the laser is all re-emitted as the new photon. If an electron scatters using a phonon before relaxing back to the valance band then the energy and therefore the wavelength of the emitted photon will be shifted due to the energy lost to the phonon.

The system considered in Raman scattering is an assembly of freely rotating, non-interacting molecules. The angular frequency of these is $\omega = 2\pi c_0 tilde\nu$, where $tilde\nu$ is the wavenumber and c_0 the speed of light in a vacuum. Incident radiation is taken to be one or more monochromatic waves of frequencies $omega_1, \omega_2$ ... which gives incoming photon energies of $\hbar\omega_1, \hbar\omega_2$ ...

Raman scattering is defined as the scattering of incoming radiation with a change of frequency ($\omega_{incident} \neq |\omega_{scattered}|$), and is the opposite to Reyleigh scattering, which is the scattering of incoming radiation without a change of frequency ($\omega_{incident} = |\omega_{scattered}|$).

Stokes law is also relevant to define here, and states that the frequency of fluorescent light is always smaller or equal to that of the light which is exciting it. Raman bands at frequencies less than the incident light frequency are called Stokes bands since they match what is expected in Stokes Law ($\omega_{scattered} < \omega_{incident}$). Raman bands at frequencies greater than the incident light frequency would violate Stokes law and are therefore called anti-Stokes bands ($\omega_{scattered} > \omega_{incident}$).

Raman spectroscopy is one method used to determine the number of layers of graphene and can give additional information about doping and defects within the graphene structure. For graphene there are 2 peaks in the Raman Spectra which are used to confirm the identity of graphene as well as being able to distinguish different thicknesses. These peaks are the G-band and the 2D-band and correspond to specific phonons associated with the graphene lattice.

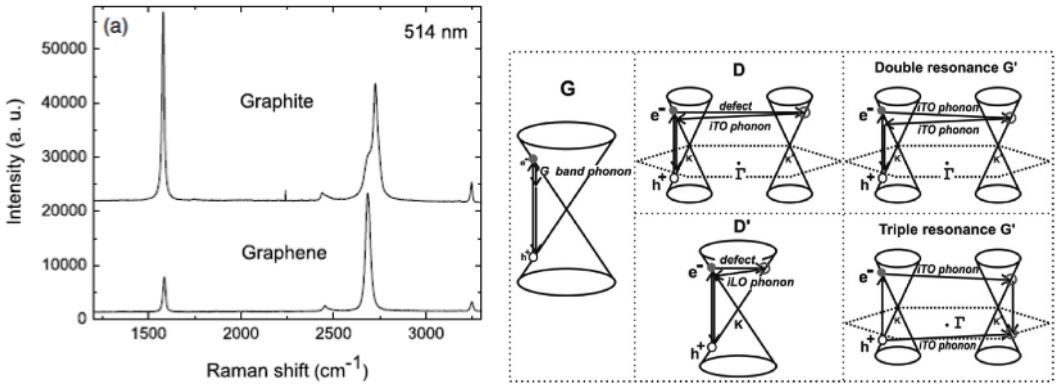

Figure 2.6: Left: Raman spectrum of graphene compared to bulk graphite with the 2D peaks scaled to the same height[7].Right: First and second order Raman scattering processes in terms of the electron interactions[8]

The G peak appears at 1,582 cm^{-1} and is associated with the doubly degenerate (in-plane Transverse Optical (iTO) and Longitudinal Optical (LO)) phonon mode. This is a first order process because it remains around the same K point (Dirac point). The electron is excited, scatters with either an iTO or LO phonon and relaxes back to the valance band. The 2D peak appears at around 2,700 cm^{-1} and is a second order process because it uses two iTO phonons to perform intervalley scattering. After laser excitation the electron is inelastically scattered across to a different K point by one phonon then scattered back to the original point before

relaxing. There are double and triple resonance processes that can contribute to the 2D peak.

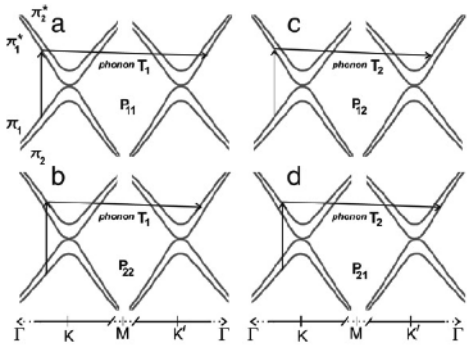

Figure 2.7: Schematics of electron dispersion in bilayer graphene[8]

For pristine FLG, Raman spectroscopy can distinguish between single and thicker layers of graphene by measuring the relationship between the intensity of the 2D-band and of the G-band. The height of the 2D-band peak is much greater than the G-band peak in pristine monolayer graphene. This is due to the extremely symmetric linear bands in the single layer which results in a triple resonance process occurring. This large 2D-band peak fits to a single Lorentzian curve with a full width half maximum (FWHM) of around 24 cm^{-1} because the triple resonance process is most favoured in monolayer graphene. In multilayer graphene the bands are no longer linear and less symmetric, which means it uses several double resonance process and different scattering events will occur. These processes are shown in figure 2.7 for bilayer graphene. Therefore the 2D peak of multilayers has a multi-peak structure. The problem with this method is that the 2D peak is susceptible to effects from doping, as well as only being able to differentiate between graphene of less than 4 layers. An alternative way of looking at the same spectra, which can differentiate between FLG up to 10 layers, compares the G peak with the first order optical phonon peak of silicon at 520cm^{-1}. The ratio of the intensity of these peaks I_G/I_{Si} increases monotonically and discretely as a function of the number of layers (figure 2.8). The G peak increases due to the additional absorption and scattering by more graphene layers, and the Si peak decreases due to the screening effect of the added graphene layers.

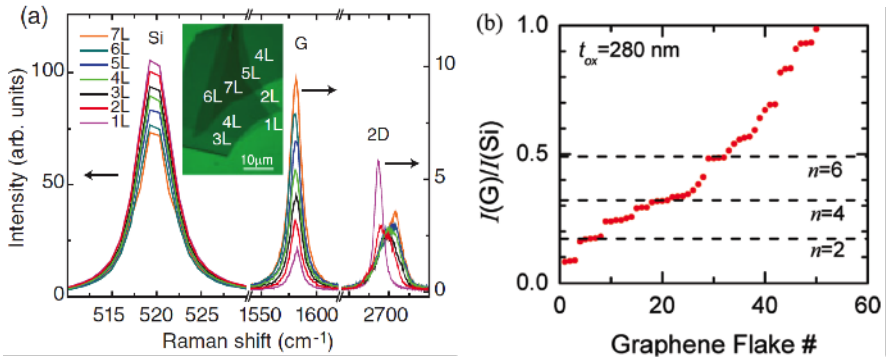

Figure 2.8: a) Raman spectra for graphene samples with different number of layers showing the change in G and Si peaks[9] b) the ratio of the G and Si peaks showing plateaus in the ratio corresponding to the number of layers for different samples[10]

2.1.5 Raman of $FeCl_3$ intercalated graphene

Iron Chloride ($FeCl_3$) is an ideal itercalation material due to it's highly electronegative Cholrine atoms which are able to affect the electrical properties of the host material. It is also a simple enough molecule, consisting of only 4 atoms, so does not present the largest challenge to incorproate beween other layers of atoms. Intercalation is characterised in stages, the stage number being the number of graphene layers in between intercalant layers. Stage 1 is when each graphene layer is sandwiched between two intercalant layers, stage 2 is when intercalated layers sandwich 2 graphene layers. The level of staging does not seem to be affected by the amount of charge transfer (large for alkali donors, weak for acceptors) between graphene and intercalant layers. The temperature gradient determines the staging of the intercalated FLG with smaller gradients resulting in a lower stage. This staging can be characterised using raman scattering, the different stages producing different peaks on the raman spectrum. This change in raman mostly occurs in the G peak which shifts from a value of $\sim$1585cm^{-1} to $\sim$1625cm^{-1} for stage 1 and $\sim$ 1612cm^{-1} for stage 2 [24].

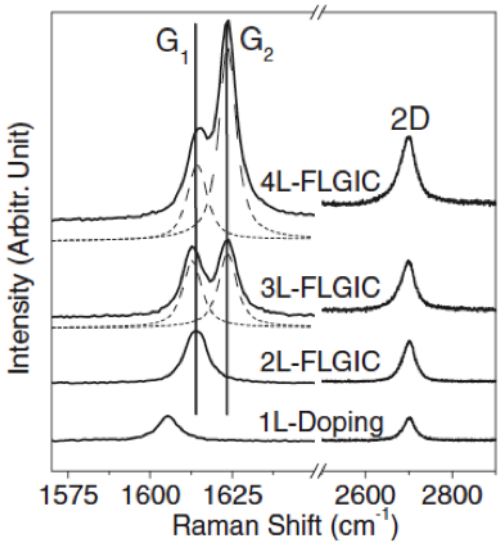

Figure 2.9: Raman plot showing change in intensity of stage 1 and 2 peaks with increasing number of layers[11]

If there is a mixture of staging in a graphene sample, the intensity of these peaks varies as a function of the number of layers. For 2L intercalated graphene, the G peak moves to 1612cm^{-1} showing stage 1 intercalation, then splits into 2 peaks for 3L and above. The stage 1 G peak intensity remains constant while the stage 2 peak at 1625cm^{-1} becomes more intense with the increase of layers. Stage 2 will dominate as no. layers increases and finally just show one peak. Another sideband at $\sim$1618cm^{-1} can sometimes be seen and is thought to be another G peak (not D or D$'$) due to nonuniform intercalation following exposure to air. The 2D peak for intercalated FLG changes from multi-Lorentz shapes to a peak able to fit just one Lorentz curve, the same as for monolayer graphene. Also the intensity of the modified peak increases with the number of layers, unlike pristine graphene. Both effects are due to a decoupling of the graphene layers in FLG due to the screening effect of the intercalant in between the layers. This decoupling means the raman signal changes to behave like many separate monolayer signals, which give the single Lorentz fit and add together to give the additional intensity dependent on the

number of layers. The decoupling is due in part to an increase in the distance between adjacent graphene layers from 3.4Åin pristine to 9.4Åin intercalated few layer graphene. The graphene layers can only couple through the intercalant molecules, and at a greater distance. The coupling between the $FeCl_3$ and the graphene is very weak due to their lattice constants being very different (6.06Åfor $FeCl_3$ and 2.46Åfor graphene). The electronic properties of intercalated few layer graphene is therefore effectively single layer graphene sheets very weakly coupled to each other, with a single dispersion near the Dirac point. As the thickness of intercalated graphene increases each layer contributes its own signal to the 2D peak, thus the 2D peak also increases.

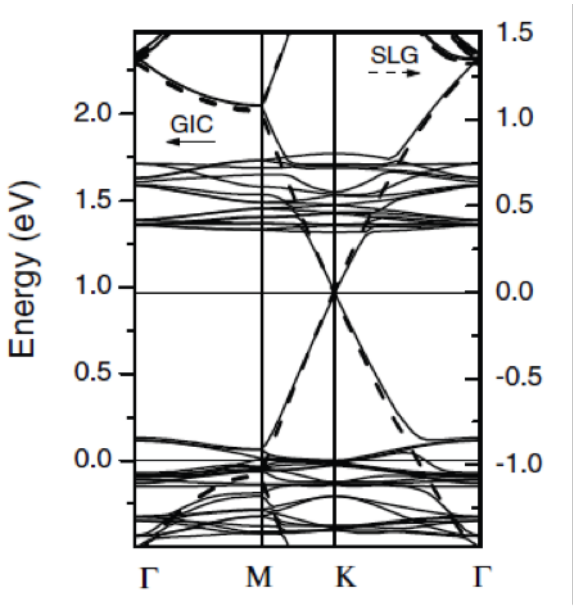

Figure 2.10: comparing the band structure of single layer graphene (dashed lines) with the band structure for graphene intercalated with $FeCl_3$[11]

If the band structure is calculated from first principles for FLG intercalated with $FeCl_3$ (see figure 2.10), it can be seen that it is very similar to SLG near the Dirac point. The additional horizontal lines at 0 and 1.5eV are mostly due to d orbitals of Iron. The main effect of the $FeCl_3$ is to shift the Fermi level and transfer charges. The Fermi energy shifts to 1eV below the Dirac point indicating hole doping. For alkali or donor intercalants, there can be a slight shift in the 2D peak position as the number of graphene layers intercalated increases. Also the G peak shifts just once rather than splitting into G1 and G2 peaks.

2.2 Plasmon properties

Graphene possesses some unique qualities that would make it useful in photovoltaic and optic based devices, including its conductivity, flexibility, and transparency. However, because graphene absorbs very little light (2.3%) it makes some of these optical applications less efficient than is desired. To increase the absorption, and therefore the interaction with light, one method is to use plasmonic nanoparticles on top of or adjacent to the graphene layer. This has already been applied with some success to graphene electrodes in a photovoltaic device with a tenfold increase in the generated photo current.

2.2.1 Plasmons

Plasmons are ripples in the sea of electrons of a conductive material. They are electromagnetic waves coupled with electrons which can travel along the surface of the material. These ripples can be excited by light or electrons. They can couple with phonons (vibrations of the atomic lattice structure) if the surface of the material is corrugated and create a resonance effect, enhancing the electromagnetic field at that point. This can be reversed as plasmons travelling along a corrugated surface can produce light. In the specific case of metallic nanoparticles, the plasmons can enhance the electromagnetic field surrounding the nanoparticle, making Raman studies, fluorescence and solar cell applications easier. In the case of Raman it enhances by creating resonating dipoles:

First the plane wave of incident light excites a point dipole with polarisability α_{np} in the nanoparticle:

$$p \propto \alpha_{np}(\omega) \tag{2.21}$$

The reradiated near field from the first dipole excites a Raman dipole in the material, with polarisability $\alpha_R(\omega_s, \omega)$ and a Stoke shifted frequency ω_s:

$$p' \propto \alpha_R(\omega_s, \omega) r^{-3} \alpha_{np}(\omega) \tag{2.22}$$

This in turn excites a secondary dipole in the nanoparticle:

$$p'' \propto \alpha_{np}(\omega_s) r^{-3} \alpha_R(\omega_s, \omega) r^{-3} \alpha_{np}(\omega) \tag{2.23}$$

The emission frequency is ω_s and the surface enhanced Raman signal from the particle is:

$$\triangle I_{SERS} \propto \omega_s^4 \int |p''|^2 dS \tag{2.24}$$

For the case of a square array with spacing L, normalised with the Raman signal without particles present, the surface enhanced Raman scattering enhancement is:

$$\frac{\triangle I_{SERS}}{I_0} \approx \frac{3}{28} \sigma Q(\omega_s)^2 \left(\frac{a}{h}\right)^{10} \tag{2.25}$$

a = particle radius, h = separation between the particle center and the graphene plane, $\sigma = \pi\alpha^2/L^2$ = the relative cross sectional area, $Q(\omega) = |\alpha_{np}(\omega)|/(4\pi a^3)$ = the mie enhancement

2.2.2 How grids excite plasmon resonance

Light scattering from a particle with a single continuous Hölder boundary is described completely by a multipole inside the particle as an infinite sum. This is the solution found by Gustav Mie (for spheroids) and extended by Richard Gans (oblate and prolate spheroids). For a nanoparticle much smaller than the wavelength of the illuminating light, it can be approximated as a dipole, with the particle being spherical. For a spherical particle located in a dielectric medium, the cross section σ_s is approximated as:

$$\sigma_s = \frac{3}{2\pi} \left(\frac{\omega}{c}\right)^4 \varepsilon_{diel}^2 V^2 \frac{(\varepsilon'_{met} - \varepsilon_{diel})^2 + (\varepsilon''_{met})^2}{(\varepsilon'_{met} + 2\varepsilon_{diel})^2 + (\varepsilon''_{met})^2} \tag{2.26}$$

ω = angular frequency, c = speed of light, V = volume of particle ε = dielectric constant, ε_{diel} = the medium the particle is in, ε'_{met} = real part of the constant for the metal, ε''_{met} = imaginary part of the constant for the metal

Resonance occurs when the real part of the dielectric constant of the metal equals twice the negative of the dielectric constant of the medium . This oscillation of the electron density is the LSPR. The scattering cross section is proportional to the volume squared (or r^6) meaning a strong dependence on the particle size. When there are no magnetic materials present (magnetic permittivity=1), the dielectric constant and refractive index are related:

$$\varepsilon = n^2 \tag{2.27}$$

LSPR occurs when

$$\varepsilon'_{met} + 2\varepsilon_{diel} = 0 \tag{2.28}$$

This means the wavelength of the LSPR depends partly on the refractive index of the surrounding medium. The real component causes a spectral shift and the imaginary part alters the width of the resonance peak. This can be used to sense the refractive index of the surrounding medium close to the surface of the nanoparticle. The nanoparticles do need to be unfunctionalised for this to work effectively. When particles are close together (<100nm), they can couple and interact assuming they behave as dipoles. This shifts the wavelength and intensity of the resonance peak and can be used to measure small changes in distance, such as a molecule sandwiched between the nanoparticles which changes length when the molecule is changed chemically. This is a known as a "plasmon ruler". A pair or group of particles can also be used to measure the rotation of a substance usually with the rotation coming from diffusion or Brownian motion. Measuring the polarisation direction, which changes as the particles rotate, does this.

2.3 TaS_2 properties

2.3.1 General properties

TaS_2 has a similar property to other transition metal dichalcogenides, which is the ability to undergo phase transitions resulting from charge density waves forming in its layered structure. This can be seen in infrared and Raman scattering below the transition temperature. New lines for amplitude and phase modes and phonons appear due to the charge-density wave formation and give information about the dynamics of electron phonon coupling in this material. These could be due to additional multi-phonon processes using condensed phonons and the hybridisation effect.

1T-TaS_2 has some interesting electronic properties, behaving like a semi conductor with a strong increase in resistivity parallel to the layers at low temperatures (less than 50 K). This is thought to be due to Mott or Anderson localization causing variable range hopping. A strong negative magneto resistance at low temperatures also supports this theory. This increase in resistivity is due to a decrease in carrier mobility rather than a decrease in carrier concentration and the effect is enhanced with additional isoelectronic impurities.

2.3.2 Raman background

Multi-phonon processes in the normal phase have broad spectra, but in the charge-density wave state they appear as sharp and strong lines because of the effect of the condensed phonons[20].

2H-TaS_2 has a transition temperature around 80 K, which means an intermediate charge-density wave.

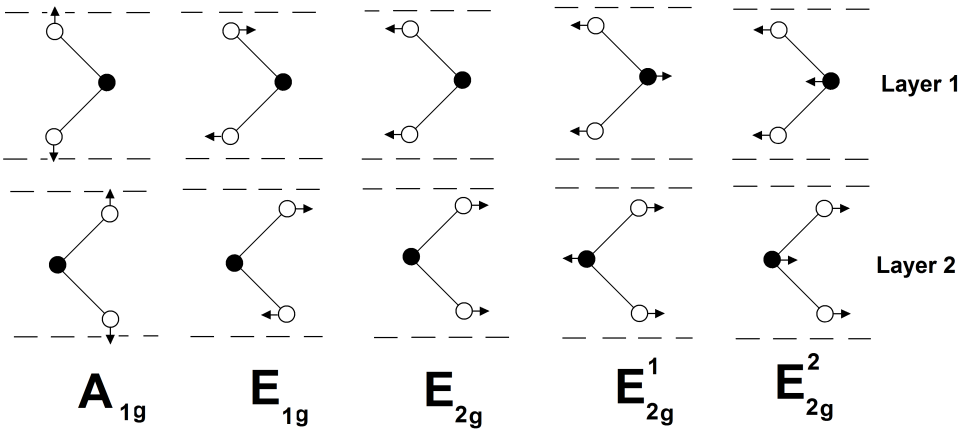

Figure 2.11: The molecular view of the different phonon modes in TaS_2, showing the movement involved with each

1T-TaS_2 shows a strong charge-density wave instability. It has two first order temperature transitions, one at 200 K from commensurate to nearly commensurate and another at 350 K from nearly commensurate to incommensurate. This also corresponds to a change in the electrical resistivity, magnetic susceptibility and reflectivity at those temperatures. In Raman studies on 1T-TaS_2 there appear 2 Raman A_g modes at 81 and 114 cm^{-1} which behave like soft phonons. When the temperature decreases past 200 K these modes shift down in wave number. Below 200 K additional Raman peaks appear due to the addition of extra phonon modes by the folding of the Brillouin zone and formation of a commensurate super lattice.

There are 4 main peaks in the 1T-TaS_2 Raman spectrum at around 100, 243, 306 and 381 cm^{-1}. This reflects the commensurate charge-density wave state at about room temperature. As the temperature is decreased the peaks intensify and split into many more peaks. The modes above 220 cm^{-1} are due to optical phonon branches and the atomic vibrations of the sulphur atoms, and the modes below 100 cm^{-1} are due to acoustical phonon branches and the atomic vibrations of the tantalum atoms. The temperature dependence of the high frequency modes in the Raman spectrum do not appear to be affected by soft phonon modes.

The same change in peaks and temperature dependence have been observed in 2H-TaS_2

2.4 $NbSe_2$ properties

2.4.1 General properties

$NbSe_2$ has two common forms, 2H-$NbSe_2$ and 4H-$NbSe_2$, where the number of $NbSe_2$ modules in the unit cell is given by the number in the prefix. $NbSe_2$ consists of a

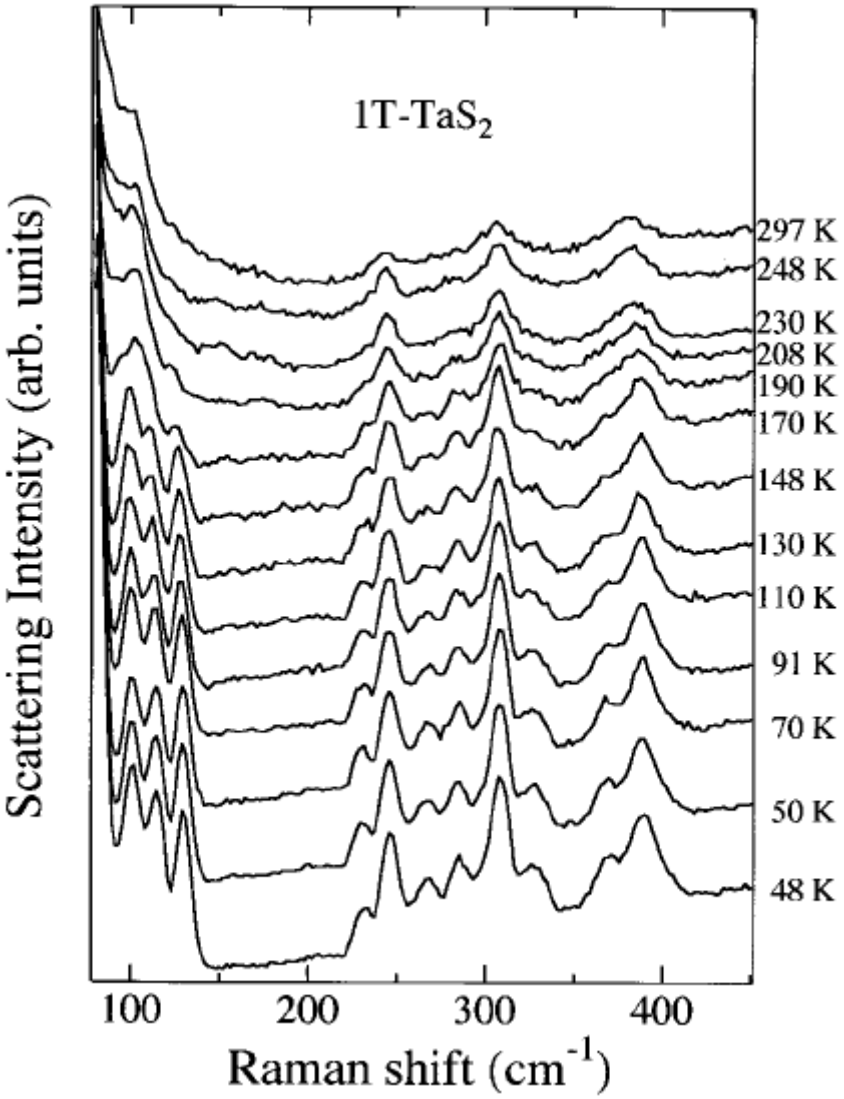

Figure 2.12: Raman spectra of TaS_2 varying temperature showing the additional phonon modes activated at low temperature

plane of Nb atoms sandwiched between two planes of Se atoms to form a molecular layer. Two of these layers form the unit cell for 2H-$NbSe_2$ arranged in AB stacking formation. The layers are easy to cleave and usually the terminating surface upon cleavage is an Se layer.

2H-$NbSe_2$ has a transition temperature as low as 33 K, making it quite a weak charge-density system. Above 33 K, without the charge-density wave, the Nb ions occupy symmetrically equivalent sites. Below 33 K an incommensurate charge-density wave appears accompanied by a periodic lattice distortion. This changes the long range order of the crystal structure and reduces the size of the first Brillouin zone. This transition is characterised with a soft phonon mode which can be seen as a harmonic variation of the amplitude of the lattice distortion, due to the addition of the charge-density wave and is usually called the amplitude mode. The energy of this mode is related to the magnitude of the electron phonon coupling constant and the temperature dependent order parameter associated to the phase transistion.

In the normal phase 2H-$NbSe_2$ has a space group D^4_{6H} and shows an incommensurate charge-density wave below the transition temperature. Below 7.2 K it also

shows superconductivity as well as the charge-density wave. One A and one E peak were observed around 40cm^{-1}, which are amplitude modes.

Condensed phonon modes and 3 phonon processes do not contribute as much as the amplitude modes and show as small or negligible in results.

(side note: an incommensurate charge-density wave is a periodic modulation of conduction electron density, whose wave length is not a simple multiple of the lattice constant)

2.4.2 Raman background

Raman spectra for $NbSe_2$ can be difficult to take because of the high conductivity of the metallic crystal, meaning that the penetration depth of the laser beam is a few hundred angstroms, which makes the interaction region very small. It also has a low decomposition temperature which means it is easily burned away by the laser if it has too much power. These problems can be overcome by using a vacuum and contact with a liquid nitrogen cold finger, or by keeping the laser power very low and allowing the sample to cool between each scan.

In $NbSe_2$ there are 3 first order Raman peaks at 29.6cm^{-1}, 230.9 cm^{-1} and 238.3 cm^{-1}. The peak at 29.6 cm^{-1} corresponds to a rigid layer vibrational mode E^2_{2g}, associated with the weak interlayer bonding. The peak at 230.9 cm^{-1} is due to the A_{1g} mode and the peak at 238.3 cm^{-1} is due to the E^1_{2g} mode. Usually for an s polarization of light the A_{1g} mode is higher in intensity than the E^1_{2g} mode and for p polarization of light the E^1_{2g} mode has a higher intensity. The A_{1g} mode corresponds to the movement of the chalcogenide atoms, while in the E^1_{2g} mode both the metal and chalcogenide atoms are moving. The frequency of these modes is therefore dependent on the square root of the mass of the corresponding atoms (or the reduced mass in the case of the E^1_{2g} mode). This means that for $NbSe_2$ the A_{1g} mode is expected to be lower in frequency than the E^1_{2g} mode.

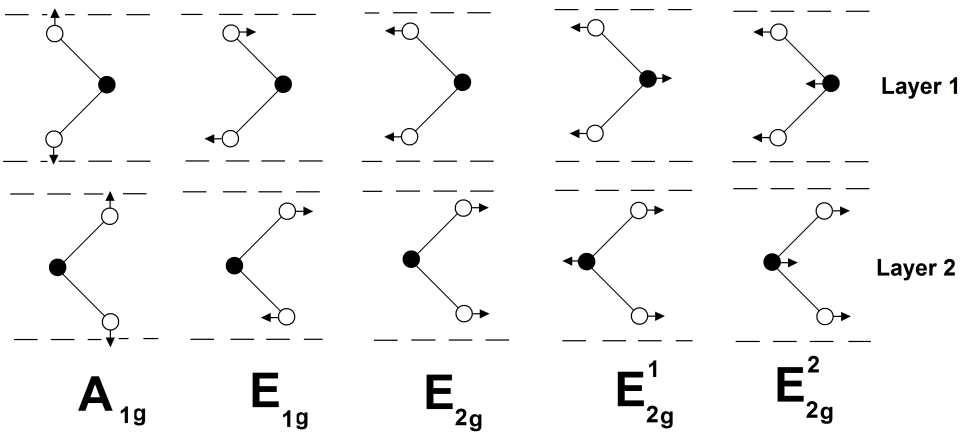

Figure 2.13: The molecular view of the different phonon modes in $NbSe_2$, showing the movement involved with each

There is another broad peak at 180 cm^{-1}, which corresponds to the presence of soft longitudinal acoustic-like phonons and the peak is a 2 phonon overtone of these modes. It is a 2 second order scattering by 2 excitations of the Kohn anomaly. The peak frequency decreases with a decrease in temperature and these soft modes condense into charge-density wave phonons. A new low frequency peak appears and

as the temperature continues to decrease it splits into two peaks of A symmetry and two peaks of E symmetry. Two strong peaks form at 49 and 82 cm^{-1} corresponding to E_{2g} and A_{2g} symmetry modes. The E_{2g} mode appears when below 122 K (transitioning from an undistorted phase to an incommensurate distorted phase) and the A_{1g} mode appears around 90 K (transitioning from the incommensurate distorted phase to the commensurate phase). There are additional smaller peaks at about 42 and 63 cm^{-1}, also corresponding to A_{1g} and E_{2g} symmetry modes respectively.

In the Raman for $NbSe_2$ there are peaks at 230 cm^{-1} and 238 cm^{-1} corresponding to parallel A_{1g} and crossed E^1_{2g} polarizations and a broad peak at 180 cm^{-1}. As the sample temperature decreases the 238 cm^{-1} peak shifts upwards and increases in intensity and the broad 180 cm^{-1} peak shifts downwards and first increases then decreases in intensity until it disappears at the transition temperature.

The low energy Raman peak, corresponding to a soft phonon mode, only appears below the transition temperature because it is the excitation of a non-zone centre longitudinal acoustic phonon.

Chapter 3

Fabrication and analysis techniques

3.1 Mechanical cleavage

The technique of mechanical exfoliation requires clean 1×1 cm wafers of substrate. The substrate consists of 285 nm of Silicon Oxide ($Si0_2$) on top of ∼1 mm of Silicon. It is important to first ensure the substrate is clean. To do this the substrates are first placed in a beaker of acetone, which is then placed in a bath of water and boiled at 100°C for 15 minutes on a hot plate. The wafers are then sonicated for 10 minutes each in first acetone, then deionised (DI) water and finally Isopropanol (IPA). They are dried with nitrogen gas and are then ready for exfoliation. The acetone cleans the substrate, the DI water removes the acetone, and the IPA removes the water and is dried off by the nitrogen. To cleave the graphite to form thinner layers of graphite, adhesive tape is used to separate the layers leaving very thin graphite sheets to place the substrate on. A small piece of the graphite is placed on one end of a strip of tape. The two ends of the tape are pressed together and pulled apart, cleaving the graphite.

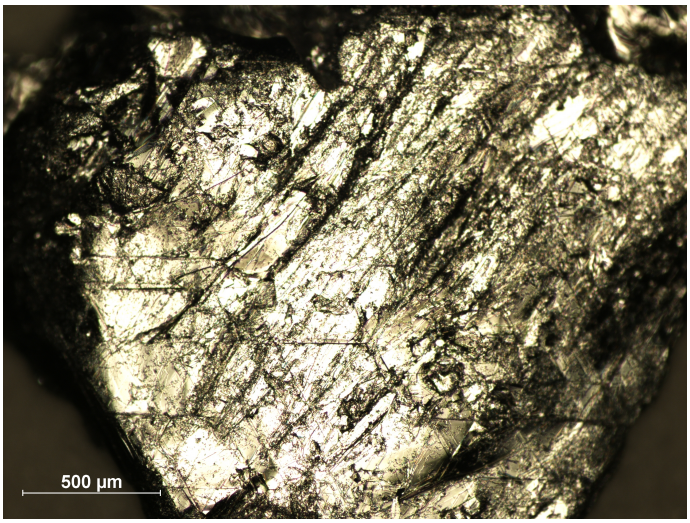

Figure 3.1: source graphite (graphenium)

This is repeated 10-15 times until this graphitic material is uniformly distributed across the length of the tape.

An optical microscope is then used to search the tape for the thinnest graphite

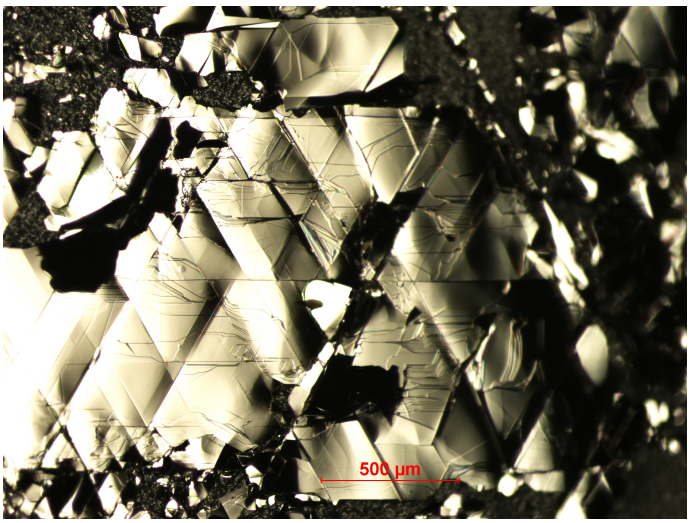

Figure 3.2: Graphite after peeling 10 times

sections (lighter grey), which can be distinguished from the thicker layers (dark grey or black). The substrate is placed on an area of tape with a high concentration of thin layered graphite for the best chance of producing a good sample of monolayer graphene. When this has been achieved the tape, with substrate attached, is placed into a plastic vacuum bag, and the bag evacuated and sealed. This is done to provide even pressure between the substrate and tape and prevent contamination. After 1 day the bag is opened and the substrates are removed from the tape carefully and briefly cleaned again. The wafers are rinsed for 1 minute each in acetone, DI water and IPA. This cleaning removes excess glue residue present due to the tape, without removing much of the graphite or graphene from the exfoliation. Then the wafers are searched manually using optical microscopes (see optical identification) to find thin layer flakes for further characterisation and device manufacture. The position of the flakes is recorded and photographs taken which can be used to measure the contrast of the flakes and therefore an estimate of the thickness of them.

3.2 Electron beam patterning

To pattern a shape onto or nearby a material being studied, first a PMMA coating is spun (to ensure an even layer) onto the substrate, then it is placed into the electron beam machine. A CAD program is used to design the pattern to be imposed on the PMMA and markers on the substrate's surface align the equipment to ensure accuracy. The electron beam then writes the pattern onto the PMMA, which is then removed from the machine and placed in a development solution, which removes the parts of PMMA exposed to the electron beam. Then with the pattern in place the holes in the PMMA can either be used to etch the exposed parts of the material to create a more useful experimental shape, or other materials such as gold or silver can be evaporated filling the holes for creating contacts, circuits, or nanoparticles on or near the material being measured.

To cut the graphene layers into a shape a reactive-ion etch (RIE) machine is used. The substrate is loaded into a chamber and the air evacuated to a high vacuum. Then a flow of argon is used to form a plasma of ions which is directed downwards onto the substrate surface. This etches the parts of the substrate and flake unprotected by the PMMA layer and leaves the remaining graphene in the

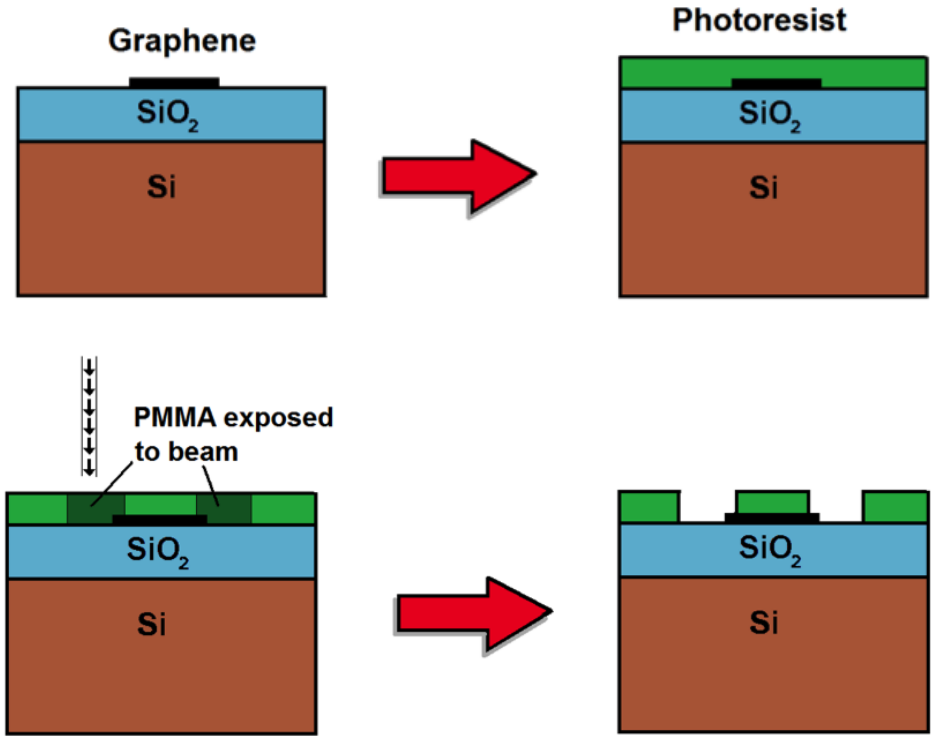

Figure 3.3: Spinning on a layer of PMMA and selectively removing it again to create a pattern for making shapes and devices around and onto a graphene flake. The PMMA is altered by the electron beam and can be developed, removing the exposed parts and leaving the rest of the PMMA layer with holes for etching or evaporation.

desired shape. The time of etching can vary slightly depending on the number of layers of graphene being etched.

To make contacts for electrical measurement, first ∼20nm of chromium then ∼120nm of gold is evaporated onto the surface in a vacuum using a thermal evaporator. The chromium is used to bind the gold to the substrate as the gold does not adhere well to silicon oxide. The gold forms the contact pads onto which gold wires can be attached. The substrate is placed in a holder mounted above the evaporation sources and gold and chromium are placed into wire baskets beneath. To prevent contamination of different sources there is a separating plate in the middle. A rotary pump is used to evacuate the chamber to low vacuum then the diffusion pump is switched on and this lowers the pressure to a high vacuum level of $< 10^{-5}$torr. Once high vacuum has been reached current is passed through each basket in turn heating the wire surrounding the source material, and melting it until a steady rate of evaporation is reached. At this point the shutter protecting the substrates can be opened and the source material forms a layer of the desired thickness on the substrate. The chamber can then be returned to normal pressure and opened. The substrates are then immersed in acetone, which removes areas of PMMA along with the gold attached to it, leaving only the chromium and gold contact pads. This is then dried using nitrogen gas.

When evaporating onto the PMMA it is sometimes useful to have two layers of PMMA of slightly different types so that the lower layer can be slightly more removed and create a cleaner edge to the deposited metal. The substrates are cut to 4×4 mm squares and placed in chip carriers. Then wires are bonded, which link the contacts on the chip carriers to the contact pads surrounding the graphene flake.

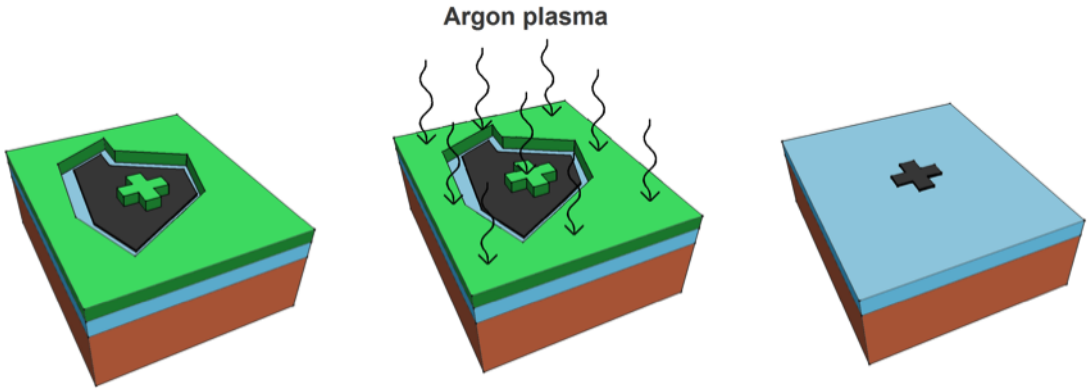

Figure 3.4: 3D model of etching a cross shape into a graphene flake using an argon plasma. The PMMA is shown in green and the graphene as dark grey. The plasma etches away at any material not covered by the PMMA protective layer.

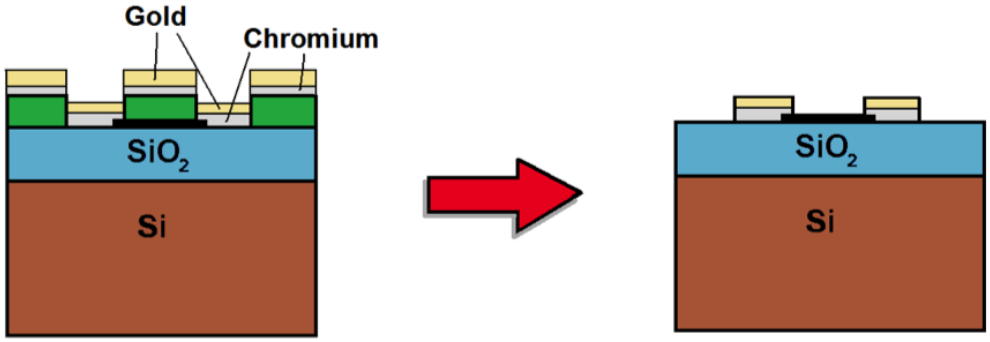

Figure 3.5: Filling the patterned holes with chromium and gold and then lifting off the excess to create contacts and (on a smaller scale) nanoparticles onto the graphene.

The device is then ready to be integrated into a circuit for transport measurement.

3.3 Intercalation

Intercalation in this thesis was achieved using the vapour transport method. The target few layer graphene sample (sitting on an SiO_2 substrate) is loaded into a vacuum tube at one end while the intercalant is loaded in powder form into the other end. The tube is sealed and pumped down to a near vacuum (10^{-5} mbar). The tube is positioned in a two zone furnace so that the temperature of the FLG is higher than that of the intercalant, creating a temperature gradient used to move the intercalant. Once heated to aufficient temperature, the powdered intercalant diffuses between the graphene layers until all available space is used up. Weak van der Waals forces then hold these extra atoms in place. Donor intercalants cause the graphene layers to expand and soften whereas the acceptor intercalants tighten and harden the carbon-carbon bond structure. For liquid intercalation (e.g. Li), the FLG is degassed and immersed in molten lithium in an argon atmosphere. $FeCl_3$ in acetone and nitro-methane have also been used as intercalants. Obtaining well staged FLG in solution is more difficult than in vapour.

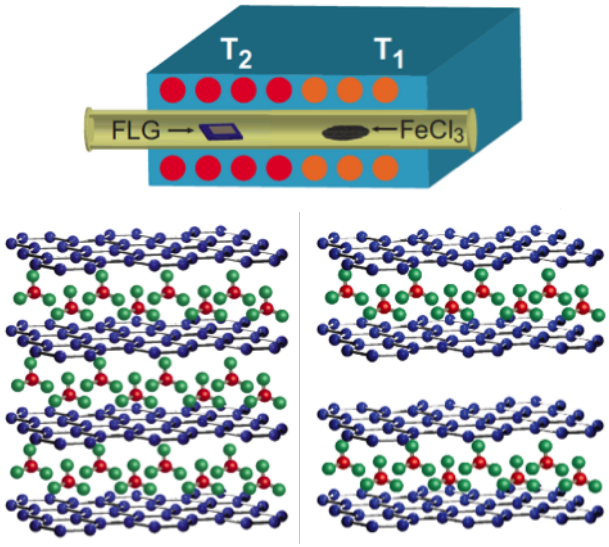

Figure 3.6: a) Two zone furnace used for intercalation of $FeCl_3$ b) stage 1 intercalation: graphene with intercalant on each side c) stage 2 intercalation: graphene with intercalant on one side

3.4 Contrast measurement

There are two well tested methods of optically determining the number of layers for a FLG sample. Firstly, optical contrast between the graphene and the SiO_2/Si substrate can be used[12], and the effect is maximised when the SiO_2 is 280nm thick using green light. The contrast is defined as the shift in intensity of the green light due to the presence of the graphene flake compared against the green intensity of the background substrate as seen in equation 3.1 [25].

$$contrast = \frac{I_{background} - I_{flake}}{I_{background}} \times 100 \tag{3.1}$$

A single layer of graphene has a contrast of about 7% with the substrate under these conditions. For FLG below 10 layers the contrast is a multiple of the value for the single layer corresponding to the number of layers of the flake, as can be seen in figure 3.7.

3.5 Dark field microscope

A dark field microscope is one where the light source is blocked off so the light is scattered before it hits the sample. It can be used to make objects with similar refractive index as the background, appear bright in comparison to that background. When the light from the microscope hits an object (usually a condenser or stop) it is scattered, and only the light scattered by the object hits the sample at a range of angles. This stops dispersed or zeroth order light (direct light source from top or bottom) from reaching the sample and only scattered light hits the sample. This forms a cone of illumination that allows the viewing of a sample in dark field.

Plasmon resonant nanoparticles scatter optical light very efficiently meaning individual particles can be observed and their spectra taken. The plasmon resonance (colour) has an effect on the index of refraction of the surrounding medium and this can be observed as a change in scattering colour in darkfield microscopy The polarization of the light can have an effect on the resulting intensity of the light in dark

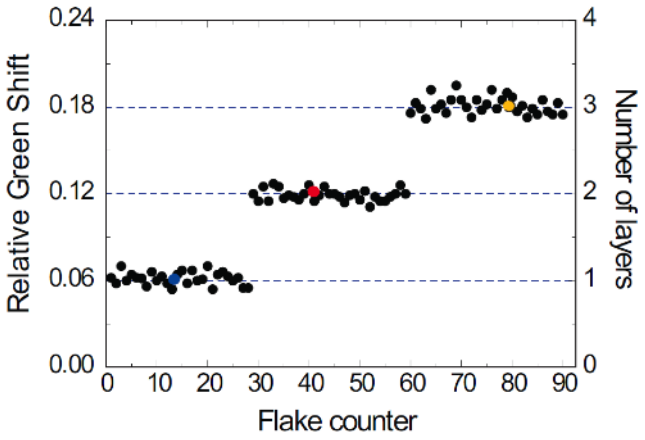

Figure 3.7: Contrast against background (Relative Green Shift) for almost 90 measured flakes. The numbered flakes are sorted and grouped by their similar contrasts, showing the relationship between number of layers and contrast for flakes on a 285nm SiO_2 substrate[12].

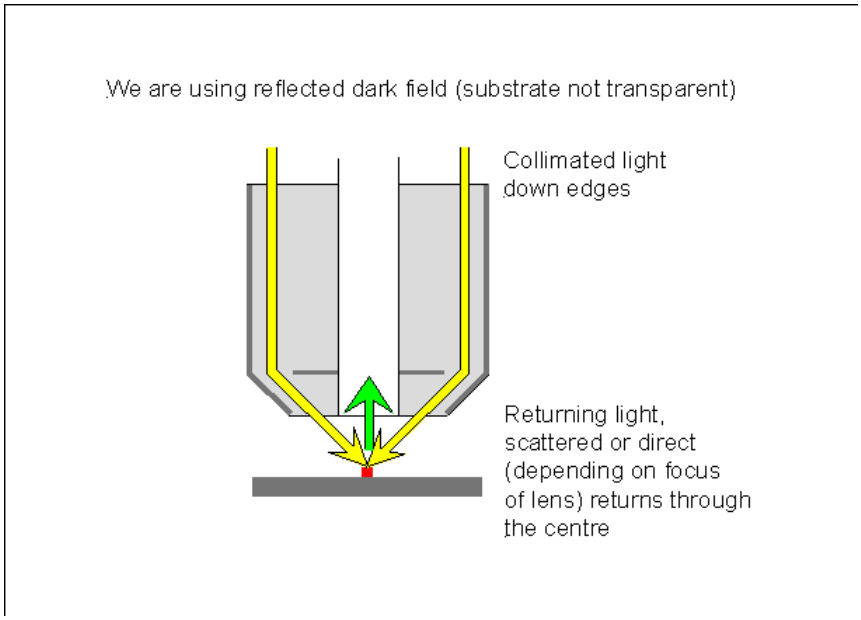

Figure 3.8: Schematic of a dark field microscope.

field. For p-polarised light (parallel to the scattering plane, or vertical compared to the surface) the scattering intensity reduces to zero when the scattering angle becomes 90 degrees, whereas s-polarised light (perpendicular (German-senkrecht) to the scattering plane, or horizontal compared to the surface) retains high scattering intensity at all angles. A dark field microscope can be combined with a spectrometer to take the spectra directly from the sample. The entrance slit for the spectrometer is aligned with the image from the microscope. For a broadband spectrum, a light source containing many different wavelengths (usually a halogen or xenon lamp) is used and is dispersed by a grating in the spectrometer before being focussed on the detector. This gives a measurement (using a 2D CCD) of spacial position on the y-axis, and wavelength on the x-axis. The particles show up as more intense regions, and the intensity profile for individual particles can be found by integrating the signal at the correct spacial position.

3.6 Raman spectroscopy

In a Raman spectrometer the wavelength of light emitted from a laser source is compared with the wavelength received at the charge-coupled device (CCD) and this is used to calculate the Raman Shift in the sample.

This produces a spectrum of Raman shift peaks produced from the sample being measured. These peaks can be influenced or additional peaks formed by changes in the electronic structure such as doping, as well as physical changes due to structural changes or defects in the molecular structure.

The laser light first travels through a pinhole to act as a low-pass filter for spacial frequencies in the image plane of the beam. Then an objective lens focuses the laser beam through two mirrors and off the notch filter to the microscope, where it is focussed on the sample. The light scattered from the sample then returns through the microscope to the notch filter. The notch filter and polariser only allows through a small range of wavelengths and polarisations which are of interest, filtering out the Raleigh and Anti Stokes light. Important in Raman studies as the shift due to Raman scattering can be so small compared to all the other scattering effects and the bulk of the laser light. The waveplate shifts the polarisation for easier detection by the CCD, then the diffraction grating bends and separates the laser light into it's component wavelengths across the CCD. This separation allows the CCD to scan across the different wavelengths and gather the light intensity associated with whichever wavelength range is needed. The CCD records the signal and passes it to a computer for decoding and analysis.

The Raman spectra given in this thesis were collected in ambient air and at room temperature with a Renishaw spectrometer. The excitation laser had a wavelength of 532 nm, focused to a spot size of 1.5 μm diameter and a $\times 100$ or $\times 50$ objective lens were used.

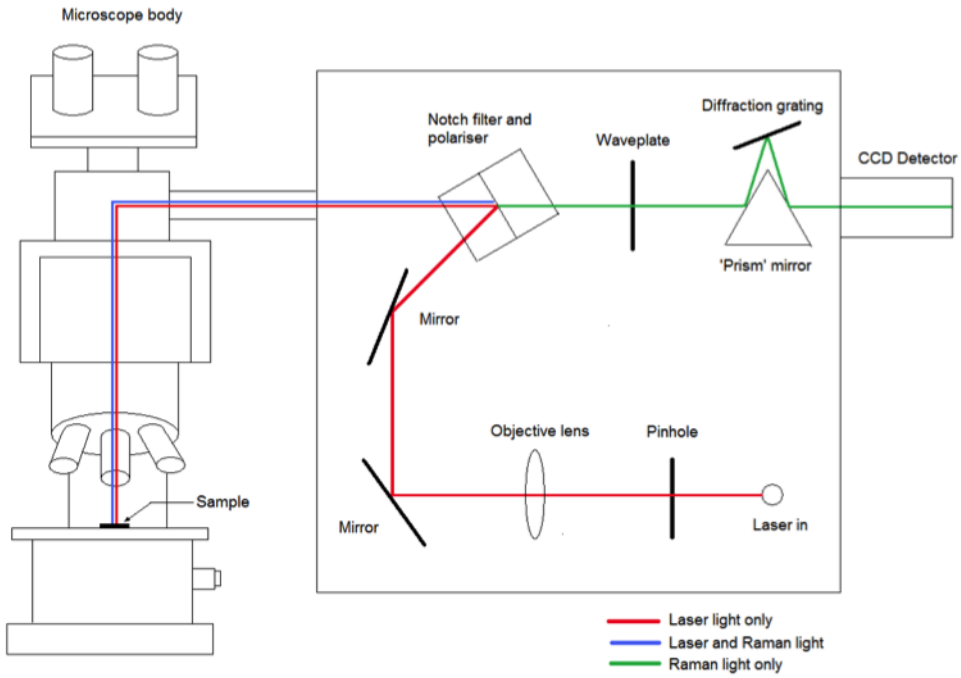

Figure 3.9: Schematic of Raman spectroscopy machine

3.7 Electrical resistance measurement

To measure the electrical resistance of the devices made using graphene, two contacts were connected as source and drain to a lockin amplifier which acted as a voltage source across the graphene. To measure the graphene resistance a reference resistor (of the order of 1 MΩ) is placed between the lockin output and the source contact with a much larger resistance compared with the average graphene resistance (which is of the order of 1 kΩ). This means that the Voltage across the two resistances (equation 3.2) can be assumed to be mainly due to the reference resistor meaning the current in the system can be approximated as being constant (equation 3.3).

$$V_{ac} = (R_s + R_g)I \tag{3.2}$$

Therefore, for the limit where $R_s >> R_g$

$$V_{ac} \cong R_s I \tag{3.3}$$

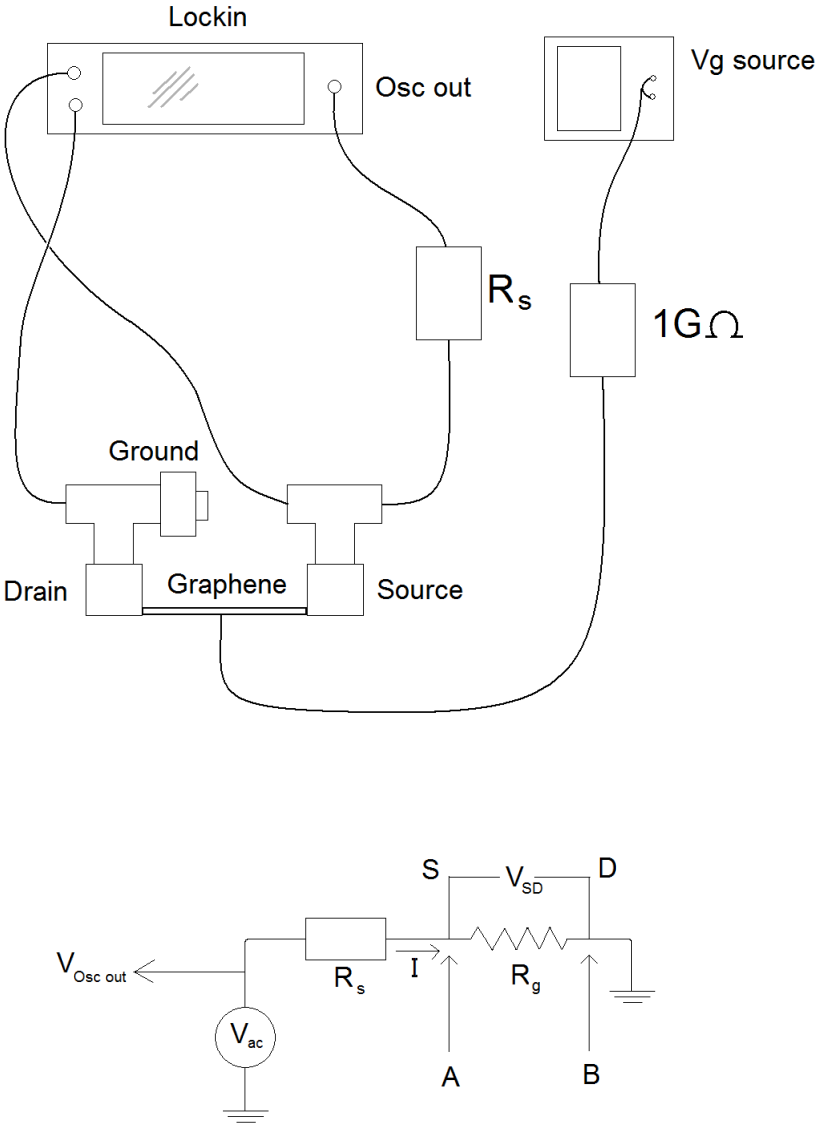

Figure 3.10: Electrical transport measurement equipment and circuit diagram

As can be seen in figure 3.10, the voltage (V_{SD}) is measured between the source and drain (A and B) and the constant current used to calculate the resistance of the graphene.

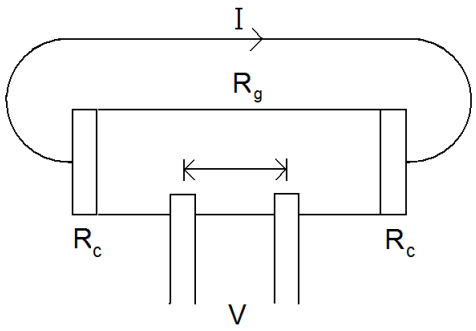

Figure 3.11: 4 terminal measurement of contact resistance

When measuring the resistance across a graphene flake the intrinsic resistance of the graphene is not the only one present in the system. Using a 4-terminal pattern of contacts it is possible to calculate the resistance of the contacts. In 4-terminal measurement, as shown in figure 3.11, a contact is placed at either end of the flake with two contacts touching the side.

A 4-terminal measurement using all 4 contacts R_{4t} yields the graphene resistance R_g and the 2-terminal resistance using just the end contacts R_{2t} gives the combined resistance of the graphene and the contacts. The contact resistance R_c can therefore be found by subtracting the 4-terminal measurement from the 2-terminal measurement.

$$R_{4t} = R_g \tag{3.4}$$

$$R_{2t} = R_g + 2R_c \tag{3.5}$$

$$R_{2t} - R_{4t} = R_g + 2R_c - R_g \tag{3.6}$$

$$R_{2t} - R_{4t} = 2R_c \tag{3.7}$$

Chapter 4

$FeCl_3$–FLG nanoribbons for interconnects in transparent and flexible nanocircuits

4.1 Introduction

One application of graphene or few layer graphene is as a component in circuits, with the advantages of thinness, transparency[6] and flexiblity[26] giving it advantages over other materials in new technologies. Examples of this include wearable electronics and flexible transparent touchscreens. This experiment aimed to increase the conductivity of few layer graphene by the introduction of the intercalant $FeCl_3$. Iron chloride was chosen because the intercalation remains stable in air and has already shown to increase the conductivity in graphene. This experiment took that further and tried to use nano shapes to show ballistic effects in this system and show that intercalation of this type is viable to act as nano-connectors or other small shapes in circuits of the future.

Graphene nanoribbons would be a good candidate for use as nano wire connections between different components[27], a concept already well tested by carbon nano tube devices. A hurdle to overcome to achieve this, at very small scales, is that the effect of edge scattering is greatly increased when the width of the conduction channel is very narrow. In a pristine and structurally perfect graphene nano ribbon a gap in electronic transport can be formed when the ribbon's width is less than 10 nm[28][27]. This is due to a localisation of edge states when the edge is in a zig zag form. The armchair shape for graphene edges does not have this localisation state, so should not produce a gap. If there is a mixture of zig zag and armchair shapes at the edge of the ribbon, then a small gap can be formed. In practice a slightly imperfect ribbon with defects and edge roughness can start to form a gap below 100 nm in width, including the formation of charge islands in the conduction channel[29][30]. This opening of a conduction gap is useful for applications such as graphene transistors, tunnel barriers and quantum dots; but for nano wires the concentration and movement of the charge carriers should be as large and free flowing as possible.

One method of improving the conduction has been to hydrogenate the edges of the ribbons by covering the central conduction channel and exposing the edges to a low power hydrogen plasma[14]. This can improve the mobility by up to 50% by removing edge scattering sites. Another method to improve the quality of produced nano ribbons is to build them out of individual molecules (e.g. 10,10′-dibromo-9,9′-

bianthryl) in a surface polymerisation forming very narrow graphene nanoribbons with an armchair edge[13]. High conductance can be reached in these ribbons with a high bias voltage to reach a delocalised state of conduction through it. A third method is to unzip multi walled carbon nanotubes, forming them into graphene nano ribbons[31]. The unzipping is done using potassium permanganate and sulphuric acid, the intercalation of lithium followed by thermal expansion, using molecular nitrogen to expand the nanotubes, the intercalation of potassium, or by longitudinal splitting using transition metal clusters. This can create polymer functionalised graphene nanoribbons which can integrate well with a polymer matrix and produce conductive and mechanically reinforced graphene nanoribbon composites. A final method is to epitaxially grow graphene nanoribbons on a silicon carbide surface[15]. The ribbon is created by etching steps into the silicon carbide and when heated the ribbon will form on the side walls of the etched pattern. This method can achieve ballistic transport in 40 nm wide ribbons at room temperature.

4.2 Experimental details

To make the few layer graphene samples, a piece of Graphenium source graphite was mechanically cleaved (see section 3.1) on a cleaned SiO_2 substrate. This created a great many few layer graphene flakes from which to draw some usable samples for Raman and electrical experiments.

It was quite important to get the order of intercalation correct. The markers used to align for electron beam patterning, as well as contacts for samples, were usually made with gold on a thin layer of chromium. This could not stand the high temperatures and etching action of the intercalant during intercalation. Tungsten and palladium were tried as replacements for the gold but it was easier to do the intercalation as the first step before markers, or to evaporate new markers onto the substrate after intercalation.

The first step was to find a stable intercalation recipe, which did not damage the graphene too much (some of the graphene was etched away or lifted off, perhaps because of a weak attachment to the substrate) and which saturated the space between the layers to give a full intercalation. This was done by iteration of temperature zones, timing and sample positioning in collaboration with PhD student Thomas Bointon. The temperature was varied to give enough evaporation of intercalated Iron Chloride, but not too much to cause lift off or damage of most materials on the substrate. Likewise the time left in both the heating phase and cooling phase were adjusted so that intercalation had enough time to occur, but not so much that crystals of intercalent grew on every piece of graphite or graphene on the substrate. The sample positioning played a similar role, determining how quickly the intercalent reached the sample and how much the intercalent affected the sample or damaged it. The final recipe which seemed to produce consistently uniform intercalation without damage can be seen in figure 4.1.

The next step was to pattern the graphene flakes into the desired nanoscale shapes using Argon plasma etching. If the intercalation was done after etching a nanoscale shape the intercalant was not present for very narrow (less than 1μm) shapes.

The intercalation changed the surface colour of the substrate, and in some cases crystals of $FeCl_3$ were formed around larger pieces of graphite present on the substrate. When the flakes were etched to shape them the original colour of the substrate could be seen in the areas where the flake had been removed.

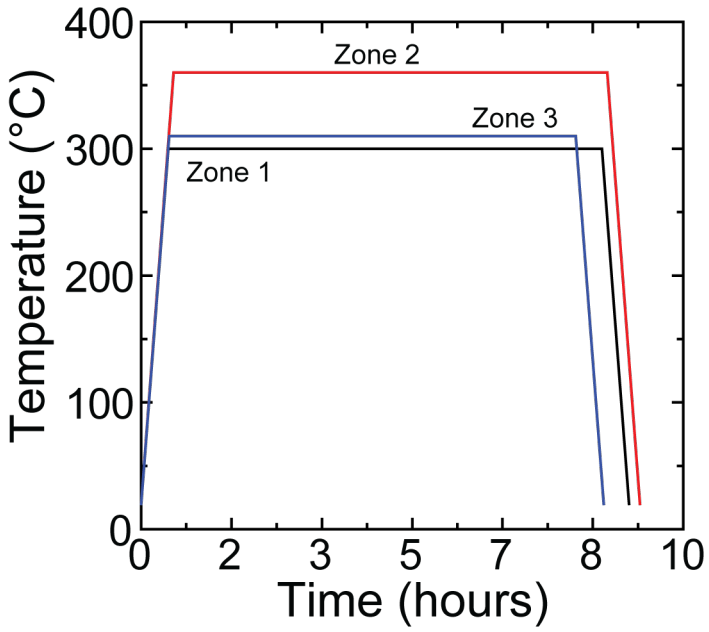

Figure 4.1: Final temperature program for the three zones of the furnace for the intercalation of $FeCl_3$ into few layer graphene. The main two zones that are important for the transfer of intercalant was zone 2 and 3

To see whether intercalation using $FeCl_3$ in a solution was possible, prepared samples of few layer graphene flakes on a silicon substrate were placed into a solution of Acetone and $FeCl_3$. When removed, a large amount of $FeCl_3$ material rested on the surface of the substrate but no change in the Raman peaks signifying an intercalation of the few layer flakes was detected. The Raman signal remained identical to pristine few layer graphene. It may be that the $FeCl_3$ powder, when suspended in the Acetone, does not have the necessary thermal energy to separate into individual $FeCl_3$ molecules and move between the graphene layers and remain there when the substrate is removed from the solution.

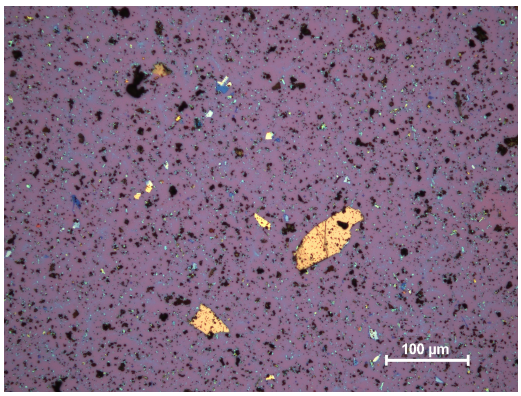

Figure 4.2: Picture of substrate after attempt to intercalate using a solution of $FeCl_3$ and acetone

Nano ribbons of various thicknesses were then etched, both in a short length for electrical transport moments, and a longer length to map the amount and quality of the intercalation procedure on such a narrow structure.

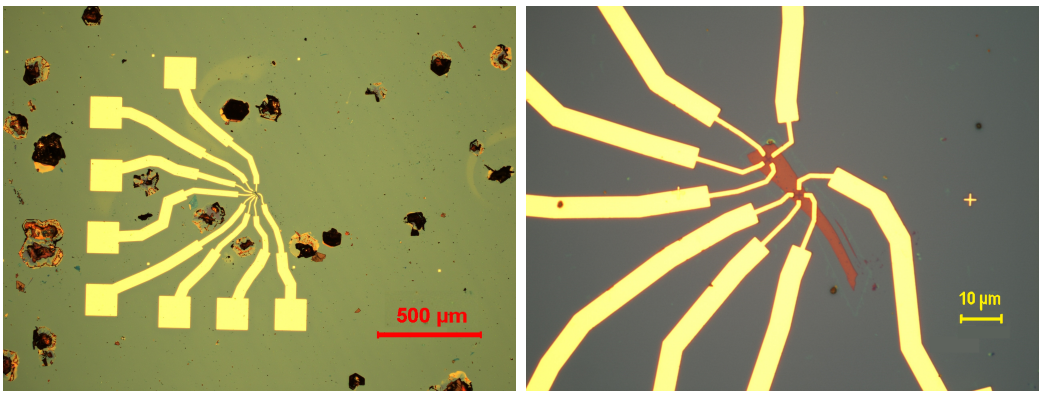

Figure 4.3: An intercalated flake, etched into two cross shapes with gold patterned to form contacts for electrical measurements. optical microsope images at a) 5x and b)100x magnifications. Also shows dark $FeCl_3$ crystals forming on surrounding bulk graphite pieces

4.3 Raman spectra of $FeCl_3$ intercalated and pristine FLG

First it was important to get some data to compare the intercalated few layer graphene to, so a short study of the Raman of pristine few layer graphene was undertaken. This has been extensively measured before by other groups and the peaks are well understood. This can confirm the quality of the starting graphene obtained from the mechanical cleavage method. This is important because the system should be largely defined by the added intercalant later, with minimal impact by impurities and defects in the initial graphene structure.

Figure 4.4 shows the Raman spectra taken of pristine few layer graphene and shows that the number of layers change both the intensity of the G peak and the shape and structure of the 2D peak. The G peak is located at 1580cm^{-1}, an undistorted single peak, with the 2D peak located around 2100cm^{-1} showing the distortions from the monolayer case. The 2D peaks changing shape is due to the increasing complexity of the band structure as seen in section 2.1.1. The G peak increases in intensity as there are more layers each contributing a response of their own. The 2D peak changes shape due to the increase in configurations possible as the number of layers increase. The number of Lorentz peaks it takes to accurately fit to the 2D peak is a good indicator of this increasing communication between the different layers. The number of Lorentz peaks needed for each fit matches the example of other groups studying the Raman of FLG.

The Lorentzian peak fitting used followed the formula:

$$y = y_0 + \frac{2A}{\pi}\frac{w}{4(x - x_0)^2 + w^2} \tag{4.1}$$

where y_0 = baseline offset, A = total area under the curve from the baseline, x_0 = center of the peak, and w = full width of the peak at half height

Figure 4.5 shows the change when the $FeCl_3$ intercalant is added between the layers. The G peak is split into two and the 2D peak can be fitted by one Lorentzian peak for all the different thicknesses. This is important as it shows the electrical disconnection or isolation between the layers, which is due to the addition of the iron chloride. This also shows the splitting of the G peak into G1 and G2 peaks, where the ratio of the peaks depends on the amount of stage 1 vs stage 2 intercalation present.

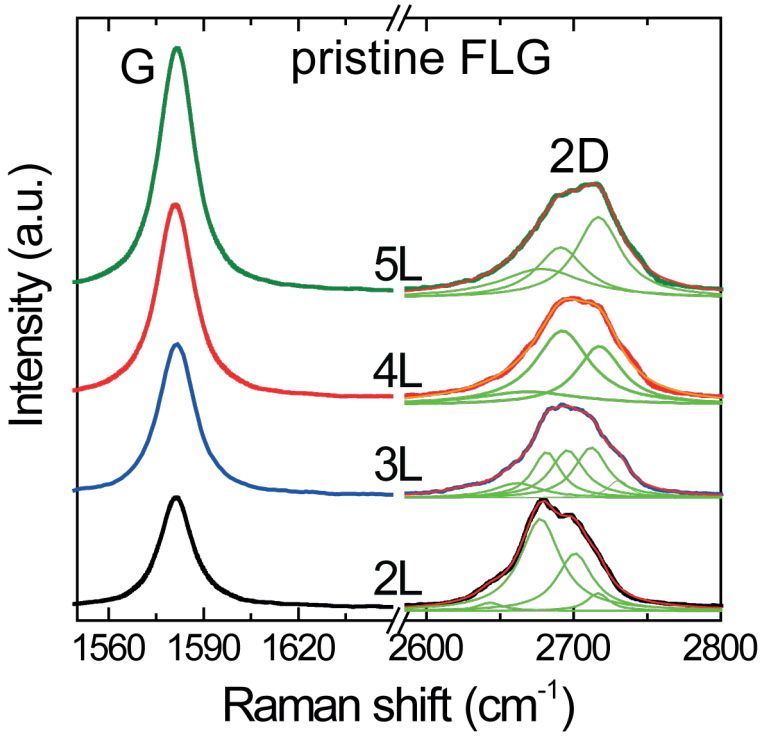

Figure 4.4: Raman spectra of few layer graphene unetched flakes, showing the G peak and 2D peak for different numbers of layers. The 2D peaks are fitted with several Lorentz peaks.

G2 in a fully intercalated system is larger because many layers are surrounded on both sides by intercalant. G1 is always present at least in a small way, because there will always be a layer of graphene on the top and bottom of the system which does not have intercalant present on both sides. If the few layer graphene has not been fully intercalated then a pristine G peak will also be present, showing there are still layers without any intercalant either side.

The intercalated graphene shows a reduced G1 peak compared to the G2 peak. This is due to the amount of graphene layers adjacent to two intercalant layers increases with the number of layers (in a fully intercalated system). The number of graphene layers adjacent to only one intercalant layer remains the same, one at the top and bottom, and so the G1 peak does not increase in intensity. For the 6 layer sample in this data, the G1 peak is probably higher due to a flake not being fully intercalated, giving more areas of graphene with wholly or partly missing intercalant layers adjacent.

4.4 Patterning intercalated FLG

Initially I tried to intercalate few layer graphene flakes after first etching them into thin structures. Figure 4.6 is an example of a cross structure with a width of 500nm widening to a micron or two where contacts could be attached. The intercalation was done using a two zone vapour recipe which was effective in fully intercalating unetched few layer flakes in previous experimental runs. When the shape was in-

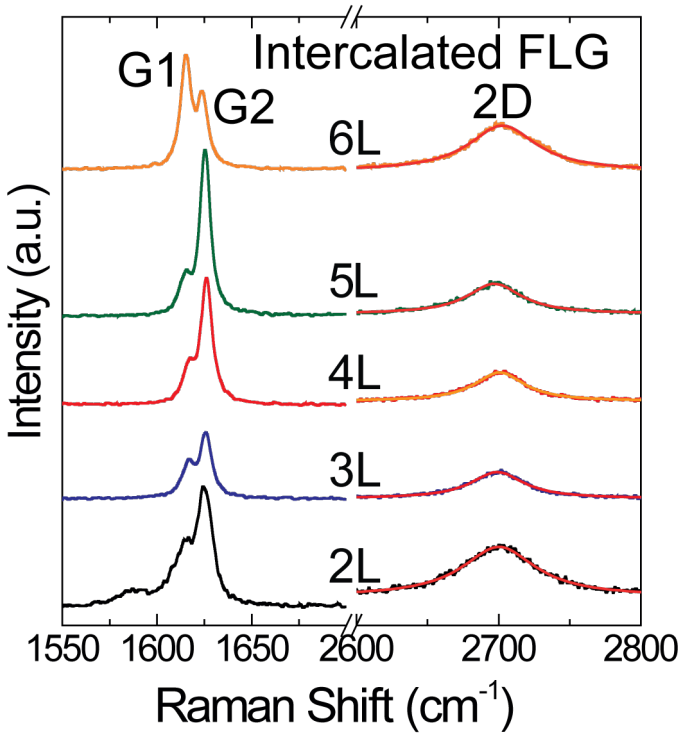

Figure 4.5: Raman spectra of intercalated few layer graphene unetched flakes. intercalation shifted G peaks and decoupled 2D peaks shown, with single Lorentz fitting on the 2D peaks.

tercalated and scanned, the central thinly etched region showed a pristine few layer graphene signal, with a single G peak at about 1580cm^{-1}. This peak was consistently pristine throughout the 500nm wide central cross regions, the peak intensity being quite low due to the thinness of the structure. In the outer wide sections of the flake the G peak is shifted and split into G1 and G2 intercalated peaks, with a very small remnant pristine peak showing that it is largely, but not quite totally, intercalated. Shapes of graphene narrower than around 1μm do not appear to retain the vapour transported intercalant after the intercalation process. There may not be enough material present to trap the intercalant molecules between the layers, at least not enough to affect a large change in properties or response.

Nanoscale shapes were then etched into flakes after they had been intercalated, rather than before, to see if the intercalant would remain between the layers in this case. The flakes were fully intercalated before etching, and remained intercalated afterwards too, showing the intercalant had not escaped from the structure this time. The intercalant molecules did not appear to have the amount of energy required to leave the gap between the graphene layers, the etching being performed at room temperature rather than in the extreme heat of a two-zone furnace. This success at intercalation can be seen in figure 4.7, with structures 200, 300 and 500nm wide all showing G peaks shifted to the intercalated G1 and G2 peak positions at 1612cm^{-1} and 1625cm^{-1}. It also shows the response of the Raman measurement to the decreasing width, with an increase of noise and the addition of an extra slope to the left hand side of the peaks, as the edges of the nanoscale structures have more impact and the amount of signal from the graphene decreases.

Raman measurements taken of 300nm and 200nm nanoscale structures were

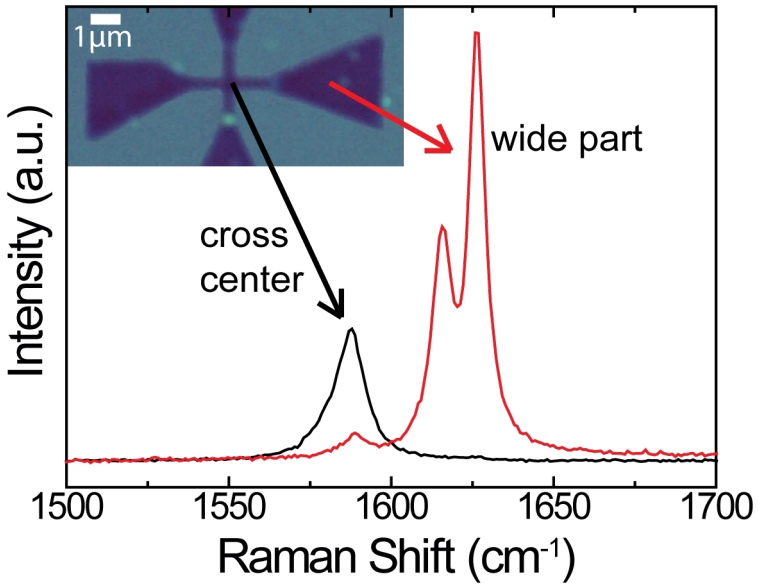

Figure 4.6: Raman spectra for the central section (500nm wide) and wide part (>1μm wide) of an intercalated cross, with the intercalatation done after etching the shape.

repeated at different times after the intercalation and etching stage, to check whether the intercalation was stable (figure 4.8). The majority of the time the samples were stored in a vacuum storage container, except while measuring, which was done in open atmosphere. The samples did not become deintercalated in that time, as evidenced by the G peaks still showing the characteristic shift to G1 and G2 positions of intercalation, at the same value of Raman shift. The peaks do vary slightly but it is probably due to the measuring spot of 1.5 μm diameter shifting slightly each time.

The 2D Raman peaks at 2700cm^{-1} for 300nm and 200nm wide nanoscale structures, fitted with a single Lorentzian peak in figure 4.9, gives another sign that the intercalant had remained within the structure and decoupled the graphene layers. Again, the signal to noise is worse in the 200nm sample due to the lack of material under the laser spot, but the shape and the fit is still close with no asymmetry or broadening characteristic of a pristine few layer system.

Long ribbon shapes were etched into an intercalated FLG flake to see the consistency of the intercalation over a long distance. The uniformity of the intercalant throughout the ribbon should be high for an application like nanowires, and it helps to prevent charge islands or nanodots forming within the ribbon length. Line scans along the length of the nanoribbons in figure 4.10 show that the G1 and G2 intercalation peaks remain both present and at the same position throughout. There was a bit more variation in the 200nm wide sample due to increased edge effects but the peaks remained consistent. This shows the uniformity of the intercalation and the consistency of the doping of the graphene by the intercalant.

The closeness of the Lorentzian fit to the data can be measured by using the coefficient of determination (r^2). This starts by calculating the total sum of squares (TSS), the difference between the mean and the data points:

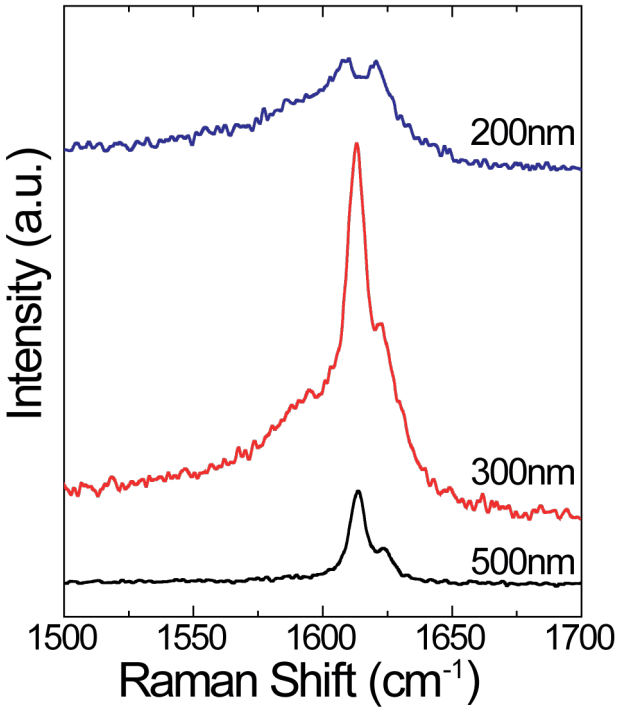

Figure 4.7: Raman spectra of the G peak of nanoribbons etched after intercalation of large scale (micron scale) flakes, for a range of ribbon widths.

$$TSS = \sum_{i=1}^{n} (y_i - \bar{y})^2 \tag{4.2}$$

where y_i = a data point value, $\bar{y}$ = mean of the data points, and n = number of data points

This can be divided into two parts, the regression sum of squares (SSreg) which is the part explained by the regression model, and the residual sum of squares (RSS) which is the part not explained by the regression model.

$$SSreg = \sum_{i=1}^{n} (\hat{y}_i - \bar{y})^2 \tag{4.3}$$

where $\hat{y}_i$ = theoretical data point from the fitting equation

$$RSS = \sum_{i=1}^{n} (y_i - \hat{y}_i)^2 \tag{4.4}$$

When the data closely matches the model, the RSS value should be very low and the SSreg value should be high. The proportion of one against the other therefore gives a good measure of the confidence of the fit to the data, which is the coefficient of determination (R^2).

$$R^2 = \frac{SSreg}{TSS} = 1 - \frac{RSS}{TSS} \tag{4.5}$$

The value of R^2 has a range of 0 to 1 so when the fit produces an R^2 value close to 1, the fit is a good one, though it is not always effective for all models or data sets.

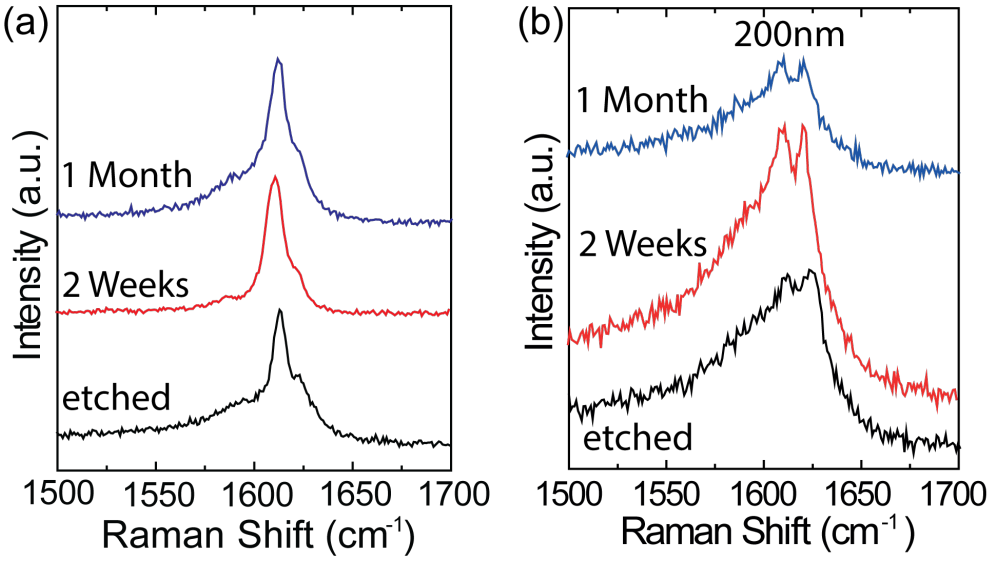

Figure 4.8: G peaks for the same location on a 15μm long intercalated ribbon for three different times: immediately after etching, two weeks after etching and one month after etching, for (a) 300nm and (c) 200nm wide ribbons.

For the data measured on the narrow ribbons in figure 4.11, the R^2 value of the 2D peak Lorentzian fit remains around an average of 0.94 for 200nm and 0.98 for 300nm. This shows the single peak fitting remains close to the data for the length of the ribbons. The 2D peak position is almost constant along the ribbon as well. Both of these support the ribbon producing a reliable single Lorentzian peak with little interaction between the layers to add additional shape or complexity to the 2D peak. This again shows that the level of intercalation is consistent throughout the ribbon, with only a slight drop in fit for the narrower 200nm wide ribbon at one end.

4.5 Electrical measurements

In a normal unetched graphene flake it is usual to see values for the resistance on the order of 6kΩ/sq. In a lithographically produced nanoribbon this can increase to much larger values (>20kΩ/sq in one study), due to the addition of edge effects and channel width reduction. For my study of resistance I produced several intercalated few layer graphene ribbons all of 1μm in length, with widths varying from 287nm to 700nm. These were measured at room temaprature in a 2-terminal setup and for flakes of different thicknesses. The 2-terminal pattern of contacts was used due the small width of the nanoribbons and the difficulty in patterning the extra contacts to only just touch the conduction channel sides. If I was able to make 4-terminal measurements of the ribbon I would have been able to measure the contact resistance of the sample and more accurately give the intercalated graphene's true resistance value.

Figure 4.12 shows the results from these ribbons, which produced values of 21.2Ω/sq to 294Ω/sq for thinner flakes (2-3 layers), and values of 34Ω/sq to 60Ω/sq for thicker flakes (5-6 layers). These are compared to some other groups' work in the plot. R_{sq} molecular is the molecular buildup of ribbons from smaller molecules, and gives a value of ~200MΩ/sq [13]. R_{sq} hydrogenated is the hydrogenation of the

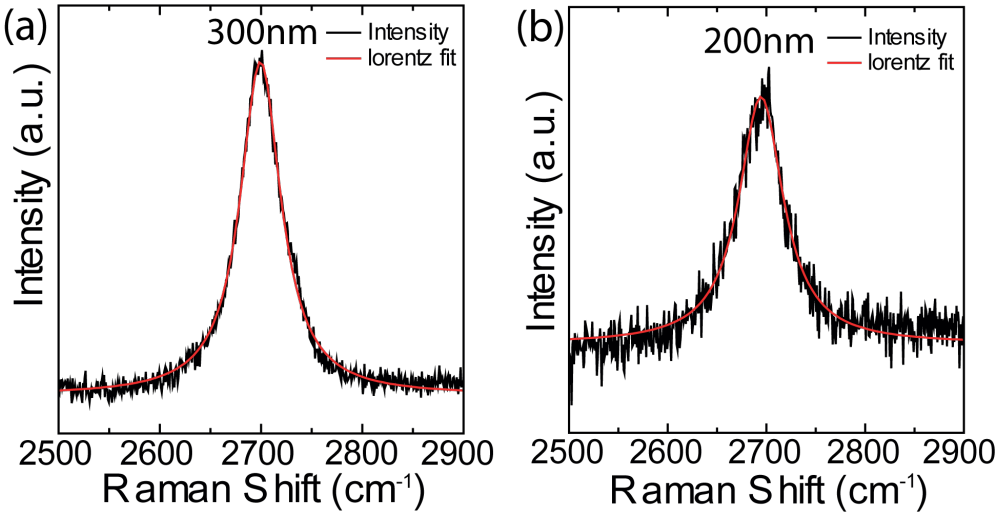

Figure 4.9: 2D peak of 15μm long intercalated ribbons for (a) 300nm and (b) 200nm wide ribbons, with a single Lorentz fit performed on each.

edges of a nanoribbon and gives a value of 92.3kΩ/sq [14]. R_{sq} epitaxial is taken from ribbons grown on the sidewalls of trenches in Silicon Carbide, giving a value of just 1.8Ω/sq [15]. The resistance values from the intercalated ribbons compare favourably to the hydrogenation and molecular techniques, but is not as impressive as the epitaxial growth. However, the epitaxial growth method is not as flexible in its applications since it is produced not flat on a substrate, but at an angle, making integration into other systems and design of devices more complex than more standard flatter techniques. It is also worth noting that the resistance values for the intercalated samples would have likely been lower if contact resistance could have been measured and subtracted from the final value.

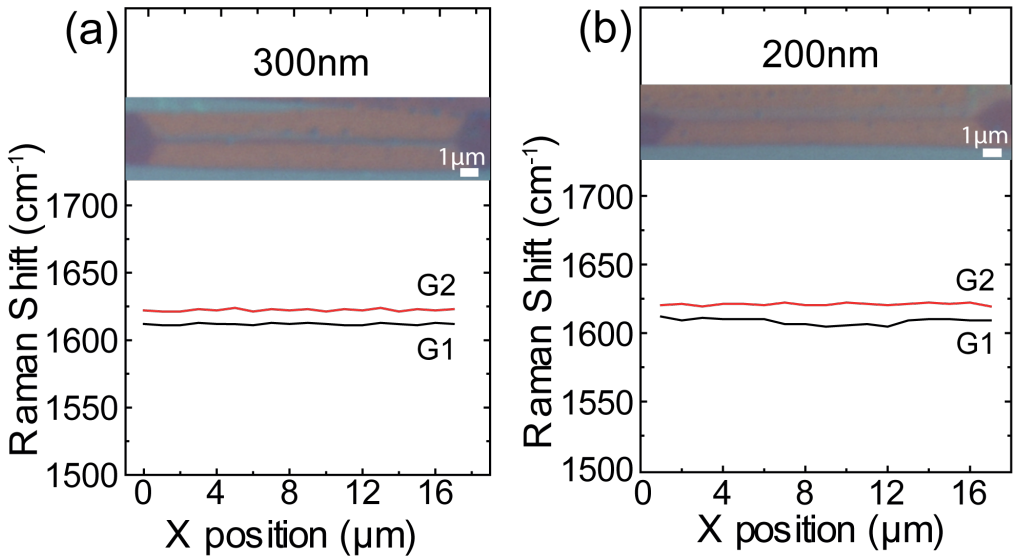

Figure 4.10: Variation of the Raman shift in the two intercalation G peaks, G1 and G2, at different positions along the length of the ribbon, for (a) 300nm and (b) 200nm wide ribbons.

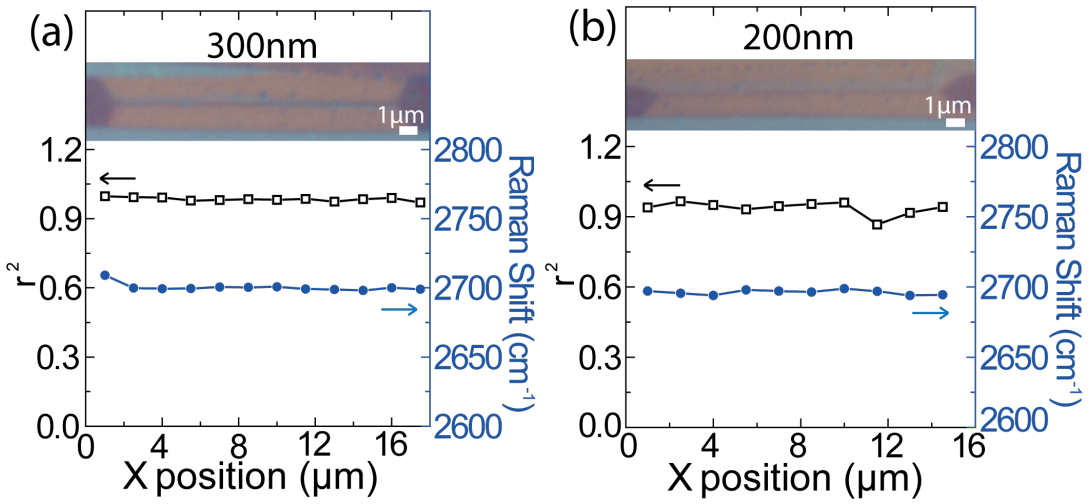

Figure 4.11: Variation in the 2D peak position (right axis) and goodness of fit (r^2) of single Lorentz curves to the peaks (left axis) at different positions along the length of the ribbon, for (a) 300nm and (b) 200nm ribbons.

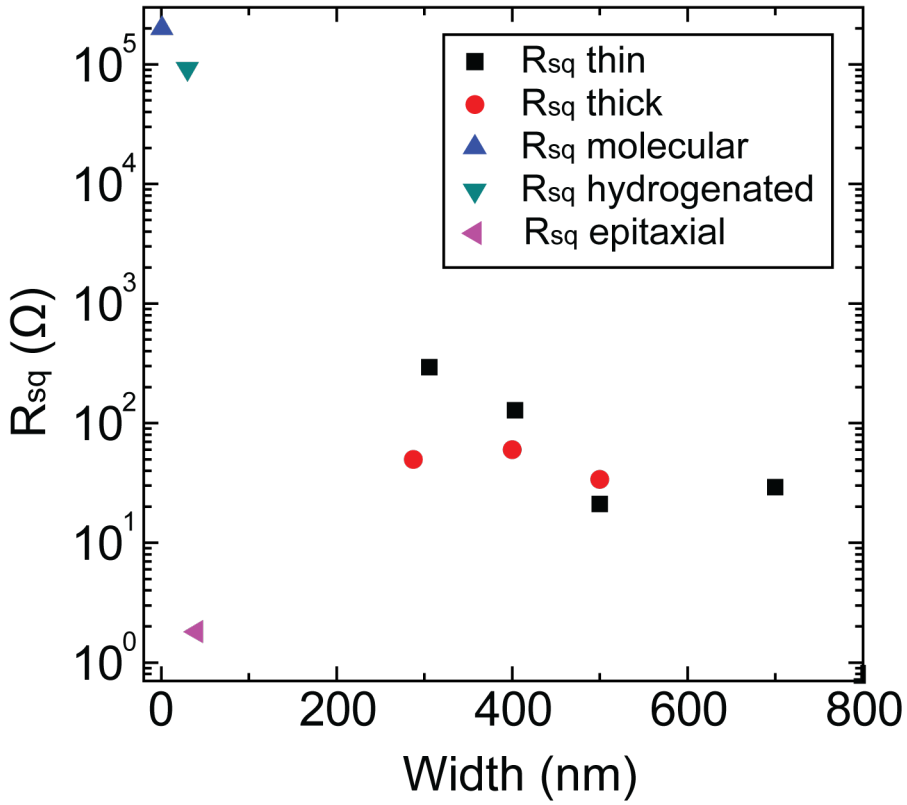

Figure 4.12: Square resistance measurements of intercalated ribbons of varying widths. R_{sq} thick consists of ribbons 5-6 layers thick, R_{sq} thin is taken from ribbons 2-3 layers thick. R_{sq} molecular[13], R_{sq} hydrogenated[14] and R_{sq} epitaxial[15] are from experiments done by other groups looking at other ways than intercalation to change the resistance of a graphene nanoribbon.

Chapter 5

$FeCl_3$ intercalated graphene as a substrate for plasmons

The plasmon modes associated with metallic nanoparticles have a wide range of applications centring around the manipulation and control of visible light into the sub wavelength range. The first application is for the treatment of cancer, where nanoshells (consisting of a dielectric core surrounded by a thin gold shell) have been used to scatter light in the near infrared to enhance optical molecular cancer imaging, and to absorb light to enable the targeted destruction of carcinoma cells using photo thermal therapy. A second application is in the enhancement of LEDs, where nanoparticle grids can scatter and slow the momentum of surface plasmon polaritons allowing more to recombine to produce photons and increasing the efficiency of the system. Another application is in data storage where gold nanorod structures can be altered in their 3 dimensional shape by a laser, using photo thermal shaping to record data and 2 photon luminescence to detect and read out the data. This 3 dimensional data recording has potential to hold far more data than a regular system. Finally they can be used in biosensing, based on either propagating surface plasmon resonances or localised surface plasmon resonances. The change in the refractive index close to the nanoparticles due to the adsorption of biomolecules can be measured in one example based on surface plasmon resonance. This particular use, as well as surface enhanced Raman spectroscopy, are the main ones which can be further enhanced with the addition of a graphene substrate.

Graphene has some properties useful as a substrate in an optoelectronic system, being transparent, conductive and thin. In combination with metallic nano particles such a system has potential for applications such as surface enhanced Raman spectroscopy and optical transmission-based localised surface plasmon resonance bio sensors. These can make use of both propagating surface plasmon resonance and localised surface plasmon resonance.

Graphene is a useful choice because of easy modification to allow more selectivity in sensors using appropriate linker molecules. Also layered structures of graphene and nanoparticles can be created to be able to view several plasmons at once.

5.1 Patterned grids with and without graphene

The aim of this chapter is to see the effect of the presence of graphene as a substrate on the plasmons produced from the metallic nanoparticles. Graphene flakes were mechanically exfoliated onto silicon/silicon oxide wafers and flakes of various thickness were identified and categorised using optical contrast and Raman spectroscopy.

Some few layer flakes were intercalated with iron chloride to see if this enhanced the plasmon resonance.

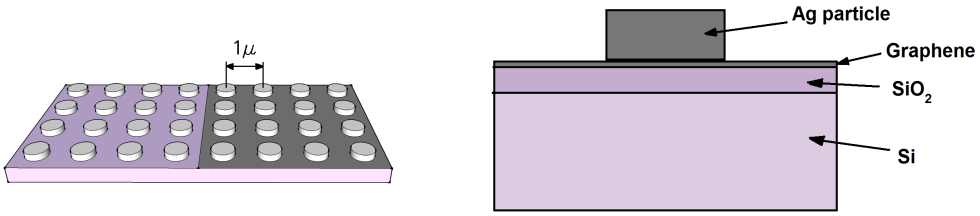

Figure 5.1: Schematic of the nanoparticles on the surface of the substrate and the graphene.

Arrays of silver nano particles were then deposited on the graphene flakes in a regular pattern using electron beam lithography, followed by thermal evaporation and deposition of the silver. The final silver nano particles were 100 nm in diameter and 50 nm thick arranged in a square lattice with period 1μm. Characterisation of the plasmon response from the nanoparticles arrays was made using dark field scattering in reflection mode. The measurement system was an inverted optical microscope with a Charge Coupled Device (CCD) camera and spectrometer. This produced a spectrum from the scattered light and allowed the spectra of around 20 nanoparticles to be measured at once.

The scattered light had a spectral resolution of better than 10 nm and was normalised using the spectrum of light scattered by the bare substrate (see equation 5.1);which was the same as the scattering spectrum from pristine and few layer graphene (without the nanoparticles present).

$$I_{norm}(\lambda) = \frac{I_{scat}(\lambda) - I_{back}(\lambda)}{I_{back}(\lambda)} \tag{5.1}$$

We started with a square grid with a nanoparticles separation of 600 nm and a nanoparticles radius of 25, 50 and 75 nm. The first attempt to pattern these on flake samples was unsuccessful because the lift off of the excess gold around the nano particles was too quick, leading to gaps in the grid and irregularities of the shape of the individual nanoparticles.

With a slower and more precise lift off we successfully created 50 and 75 nm grids. When these grids were measured using the dark field microscope, the intensity peak measured was much smaller and cut off compared with the peak expected for a plasmon resonance. This was probably due to reaching the diffraction limit of the grating, so we increased the spacing of the nanoparticles to 1 micron.

However the larger grid spacing did not help to increase the sharpness of the peak very much so we decided to use silver instead of gold for the nanoparticles. The silver made a much sharper peak, giving a much stronger plasmon resonance. The peaks did not scale with the particle size when measured for different grids. The resonance was expected to increase with an increase of particle size [32] but the peaks remained about the same value.

It was thought that this could be due to the SiO_2 layer or impurities in the graphene. The substrates were annealed to try and remove any impurities from the

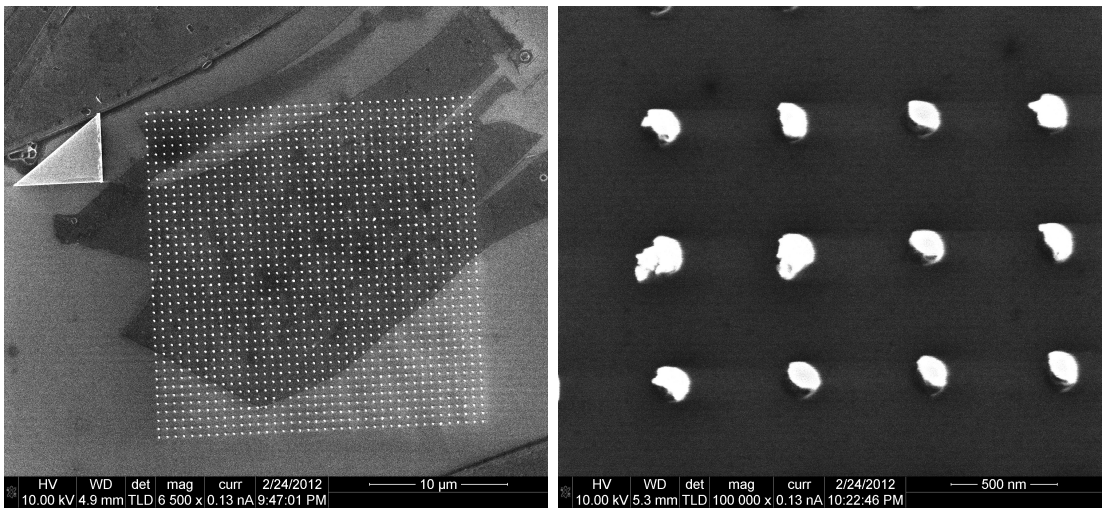

Figure 5.2: Scanning electron microscope images of the first attempts at a nanoparticle grid evaporated onto graphene. This example had a lift off too fast to give a uniform round shape to the particles, and leaving gaps in the grid pattern.

system. When the annealed grids were measured the intensity was reduced slightly but the same constancy of intensity, despite particle size, was still seen.

Then the effect of the thickness of graphene was tested using 50 nm nanoparticles radius grids.

The silver nanoparticles grids were measured using an SEM to determine their uniformity. They were not perfectly uniform but probably sufficient for the purposes of the experiment.

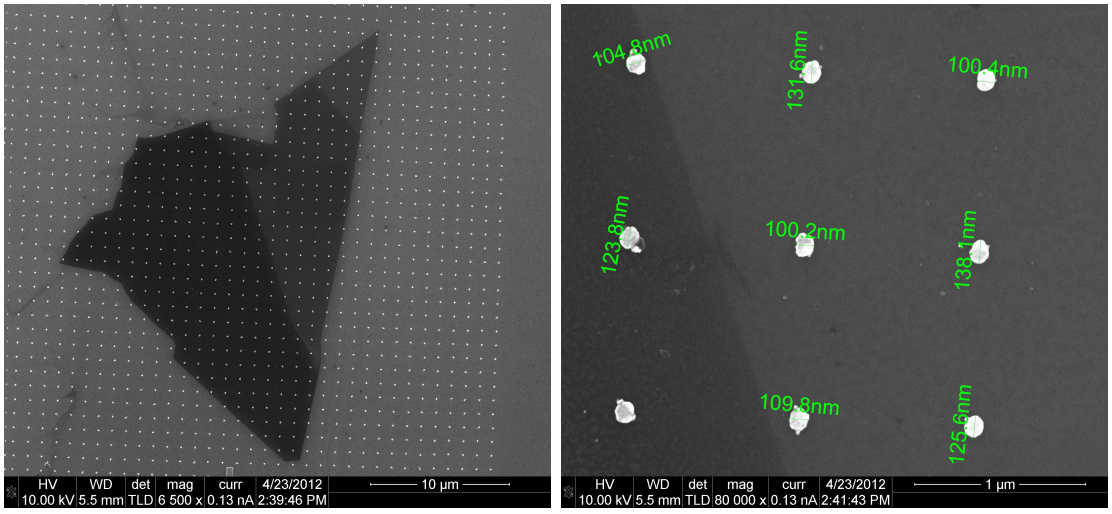

Figure 5.3: Scanning electron microsope images of one of the final grids of silver nanoparticles patterned and deposited onto a graphene flake. a) Different thicknesses of the flake from ∼10 layers (darkest shade), to 2 layers (medium shade), to a single layer (lightest shade), and surrounded by the substrate. b) A close view of the individual particles showing a fairly round and uniform shape to them.

The normalised dark field scattering spectra for arrays of nanoparticles on both pristine and intercalated few layer graphene were measured first. A broad peak centred around 530nm is present for both pristine and intercalated graphene and as the number of layers increases the attenuation (reduction in intensity) increases,

making the peak decrease in size. The amount of attenuation is greater for pristine graphene than intercalated graphene. It might be expected from previous studies [33] that increasing the thickness of the graphene would also increase the effective refractive index close to the particles, this would give a red shift to the spectral position of the plasmon resonance. The resonance peak does not shift in the data, only decreases in intensity and the doping of the intercalant does not change this. This can be explained by the thinness of the additional layers, around 2nm for 6 layers of graphene, which is much less than the optical field penetration depth associated with localised surface plasmon resonances [34].

The strength of the scattering and the change in the intensity of the peak could be explained by the graphene affecting the reflected optical field. This reflected field interferes with the incident field modifying it and therefore modifying the scattering process. Each additional layer alters the field a little more.

5.2 Raman study of intercalated and non intercalated particle grids

The Raman characteristics of the graphene should increase in intensity when due to an additional signal from the nanoparticle grids. As seen in figure 5.6 the intensity of all layers from 1 to 6 are increased due to the presence of the particles. The exception is the single layer which is probably due to the flake with no particles measured being several layers thick. Even with the added particles intensity the single layer does not increase by enough to be greater than a multilayered flake.

Both the dark field scattering data and the Raman spectra shows there is a response to the addition of graphene as a substrate. The Raman spectrum shows there is an increase to the signal with the presence of particles on the surface.

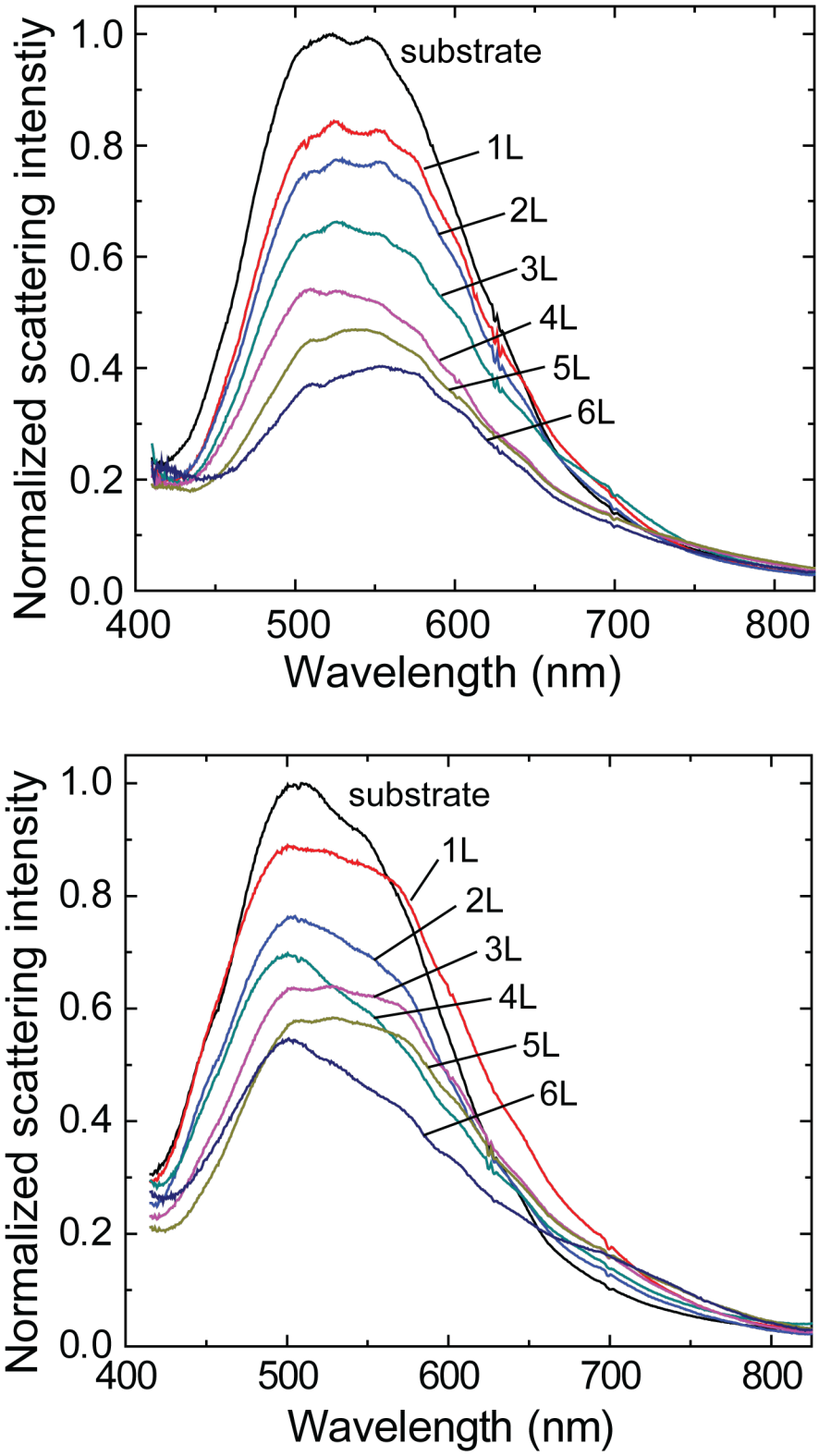

Figure 5.4: Scattering spectra of a) pristine and b) intercalated graphene of different thicknesses with particle grids on top, and includes the signal from the bare substrate.

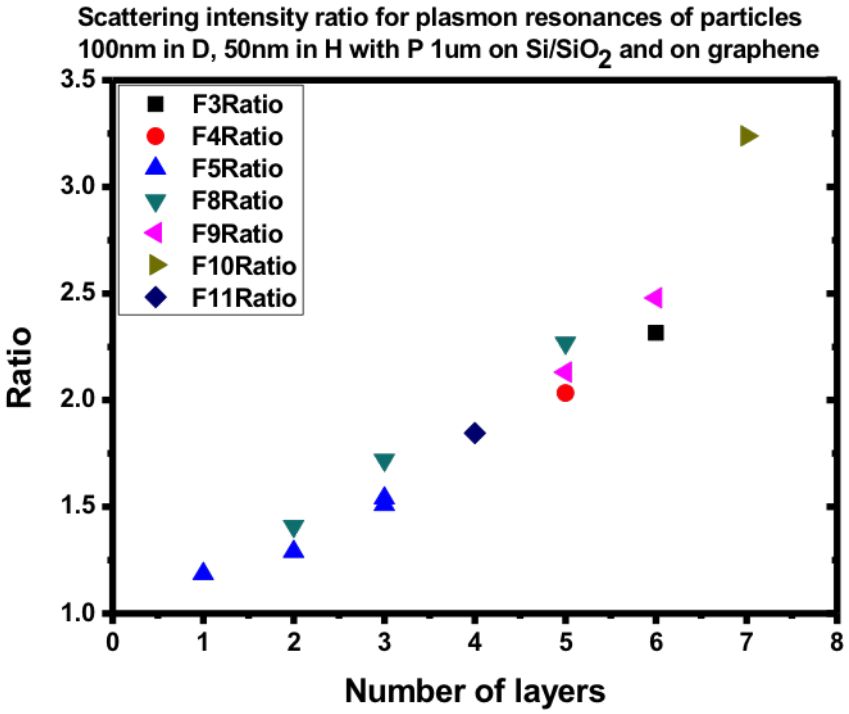

Figure 5.5: Ratio of intensity of plasmon resonance of nanoparticles with graphene and without (just the SiO_2/Si substrate background).

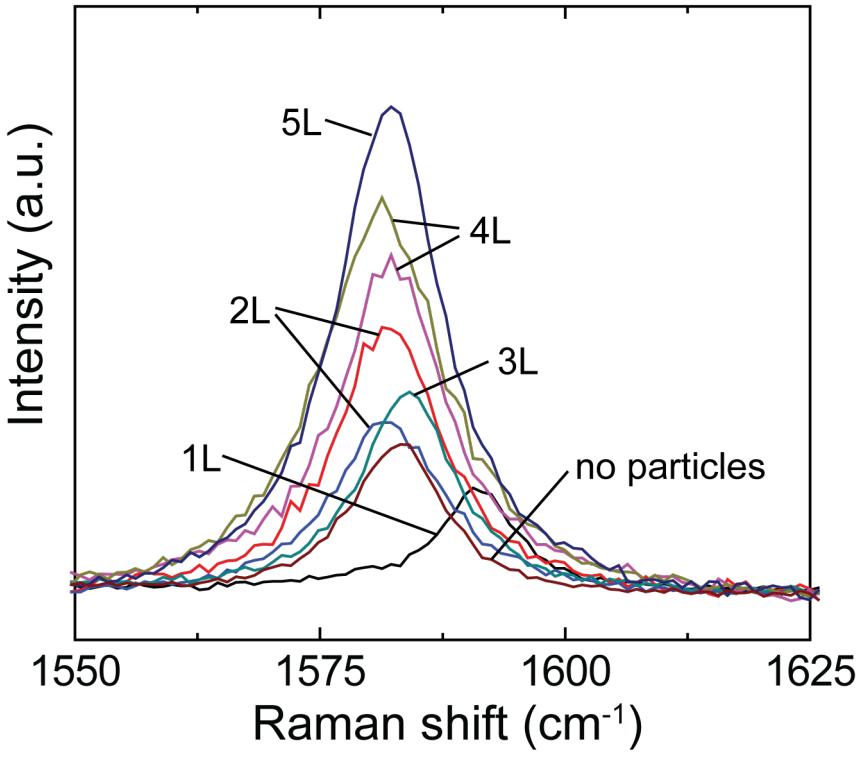

Figure 5.6: Raman comparison of pristine flakes of various thicknesses with particles on top to a flake without particles on top.

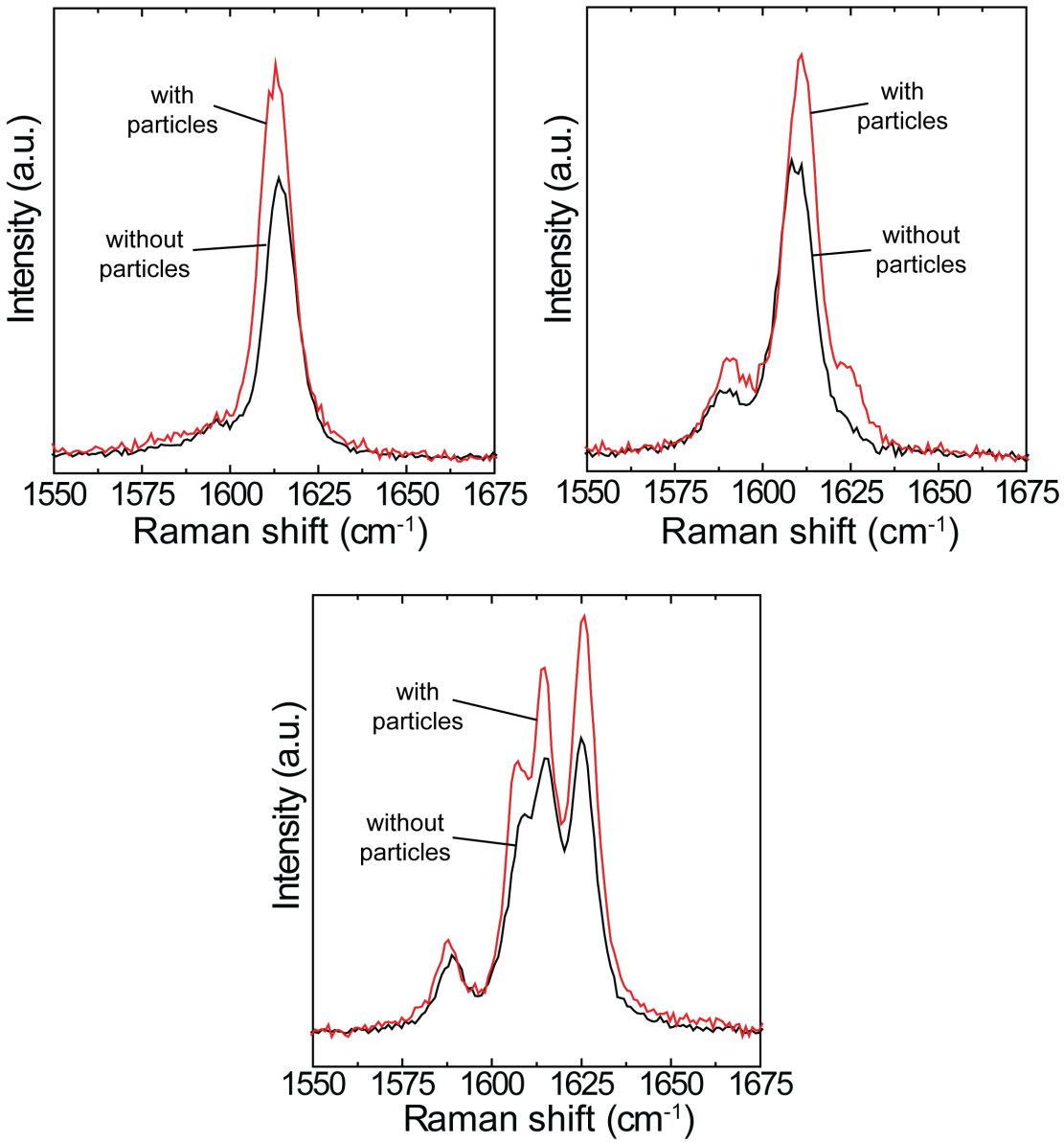

Figure 5.7: Comparison of intercalated flakes before and after nanoparticles were deposited on top for three different intercalated flakes.

Chapter 6

Few layer Raman study of 1T-TaS_2

As discussed in chapter 2 TaS_2 has a range of unique properties such as charge wave density causing phase transitions and electronic properties at low temperature. However not all the intrinsic properties of this material are known. Some Raman studies on this material, such as by Hajiyev et Al. have been done [35], but in particular an accurate method to determine the number of layers in few layer TaS_2 is missing. This chapter is focussed on the Raman studies of few layer TaS_2 in order to provide a method for determining the number of layers. In addition the Raman studies for few layer samples could provide some interesting properties, especially if these can be controlled with selective etching of the TaS_2 into patterns or conduction channels.

6.1 Contrast

First a study of the characterisation of TaS_2 via optical contrast with the surrounding substrate. The contrast forms a similar linear pattern as graphene, with plateaus where flakes with the same number of layers also share similar contrast values. Each layer contributes an additional contrast percentage, which in this case seems similar to graphene as well, about 7-8% per layer. This is consistent with a layered material where each layer absorbs a portion of the light.

6.2 TaS_2 Raman response for different thickness

The response for different flake thicknesses was examined. It was necessary to use a very low laser power and short exposure times because heating from the Raman laser caused the layers to etch away. This became a focus of the experiment, to find out the effect of the etching on the material. In figure 6.2 the substrate background is subtracted from the data to give clearer peaks There were 3 major peaks found in the spectrum caused by the TaS_2 layers at $\sim$180cm^{-1}, $\sim$290cm^{-1} and $\sim$400cm^{-1}. All three peaks decrease in intensity with decreasing layer number until 2 layers thick, where the peaks disappear and the sample reads the same as the substrate peaks, giving a flat plot when the substrate background is removed. The peaks due to the SiO_2 substrate is shown at the bottom of the graph.

All three peaks increase intensity at the same rate as the number of layers increases. This can be seen in figure 6.2 All represent optical phonon branches where the increased number of layers increases the overall number of molecules vibrating to produce those modes.

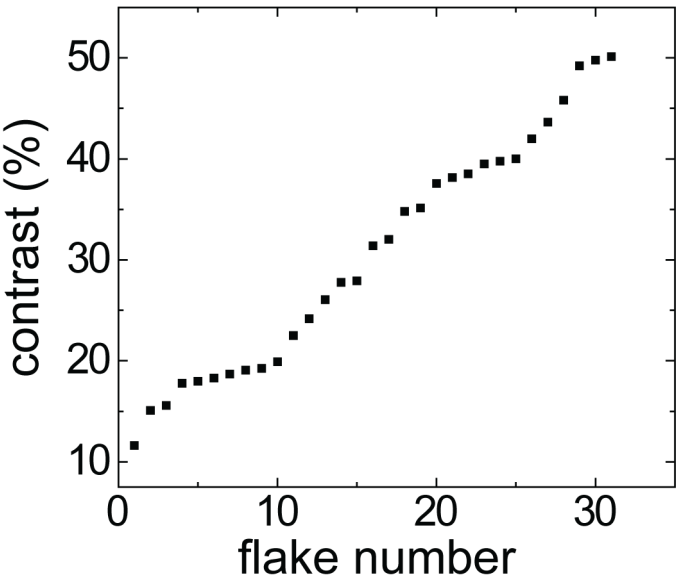

Figure 6.1: Optical contrast measured in the green spectrum for flakes of TaS_2 of various thicknesses.

Scanning one TaS_2 flake 3 times successively at a laser power of 10% at a single point produced a reduction in intensity of all peaks, as seen in figure 6.4. This starts to approach the line for the substrate, but the TaS_2 peak at 400cm^{-1} remains a most prominent feature meaning that the flake is still there but reduced in layer thickness.

6.3 Raman response to etching of flakes

To test the effect of etching on a larger scale, the TaS_2 flakes were scanned with the Raman laser on 10% power for 30 seconds at multiple points on the flakes, mapping out a large area and reducing the thickness of the flake uniformly. We hoped that the flake could be etched away a few layers at a time, leaving a thinner surface, the thickness of which could be controlled by the time and power of etching. To measure the Raman signal of the flake without etching any further the scans were done using 1% power for 10 seconds. The amount of noise from this short scan was quite high, but could be reduced by repeating the measurement several times with a gap of at least 10 minutes between measurements to let the material cool.

When the flakes are etched the peaks reduce in intensity until there is no Raman signal that can be detected above the noise level. There is still a contrast difference with the substrate but the Raman signal matches the background substrate signal almost exactly. This suggests that the flake has been etched away entirely leaving an impression of the flake on the surface of the substrate. The area etching failed because the material was too sensitive to the prolonged exposure to the laser. Further steps to prevent this could be to try and adjust the laser intensity and timing to reduce the amount of heating. In principle and from the earlier Raman scans in figure 6.4 it should be possible to etch layers effectively and pattern them into device shapes.

These studies have shown that the number of layers is indeed reflected by the Raman spectrum and that the etching of TaS_2 into areas or shapes may be possible

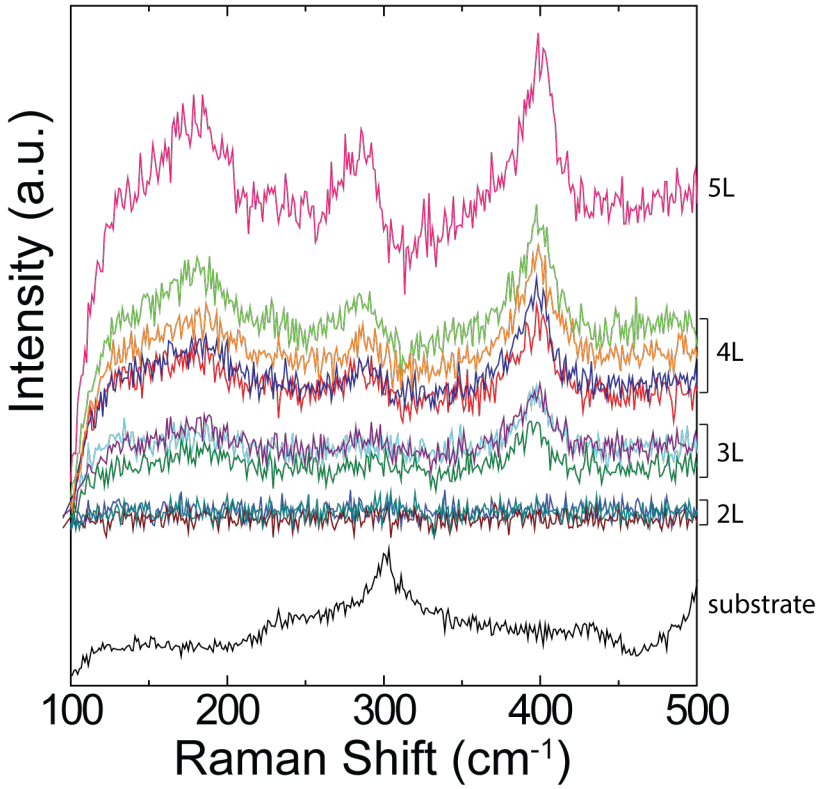

Figure 6.2: Raman spectrum of flakes of varying thickness of TaS_2.

if the power and timing of etching can be perfected and controlled precisely.

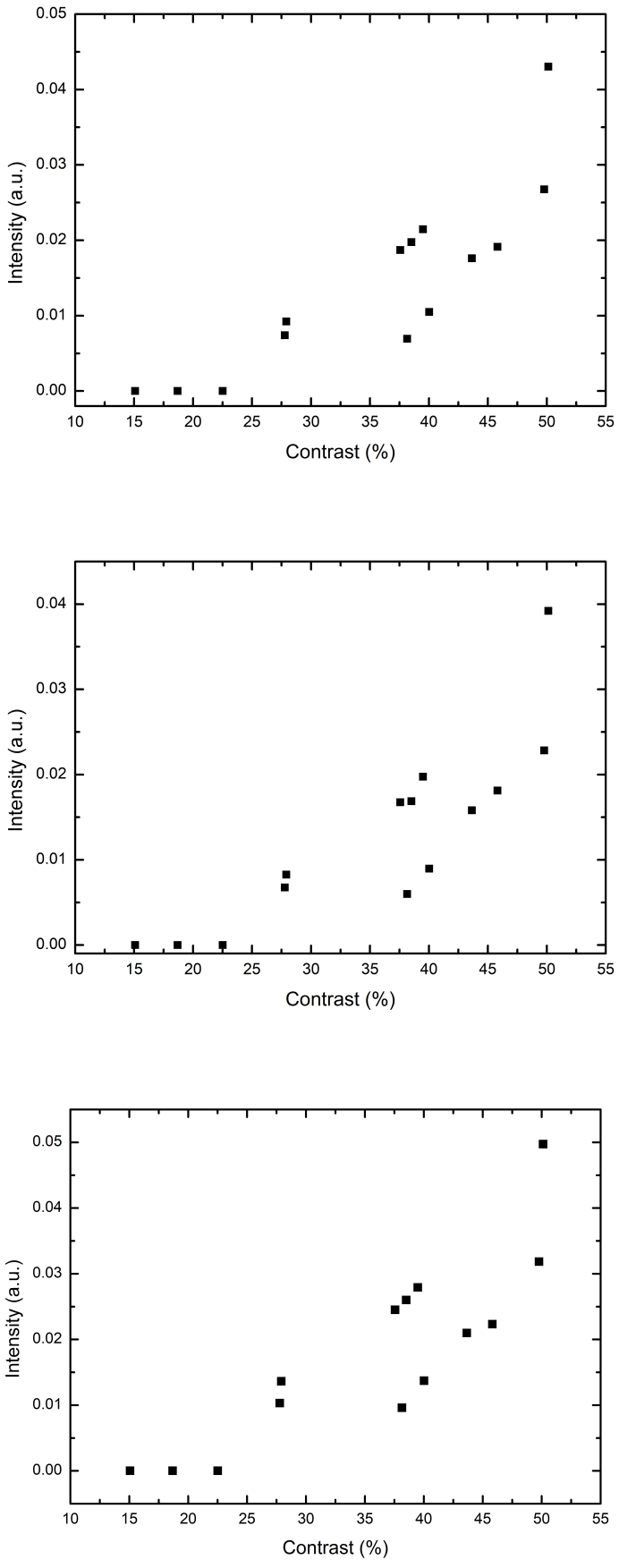

Figure 6.3: Peak intensity vs contrast for different peaks of the TaS_2 flakes. a)peak 1 at 180cm^{-1}, b) peak 2 at 290cm^{-1}, c) peak 3 at 400cm^{-1}.

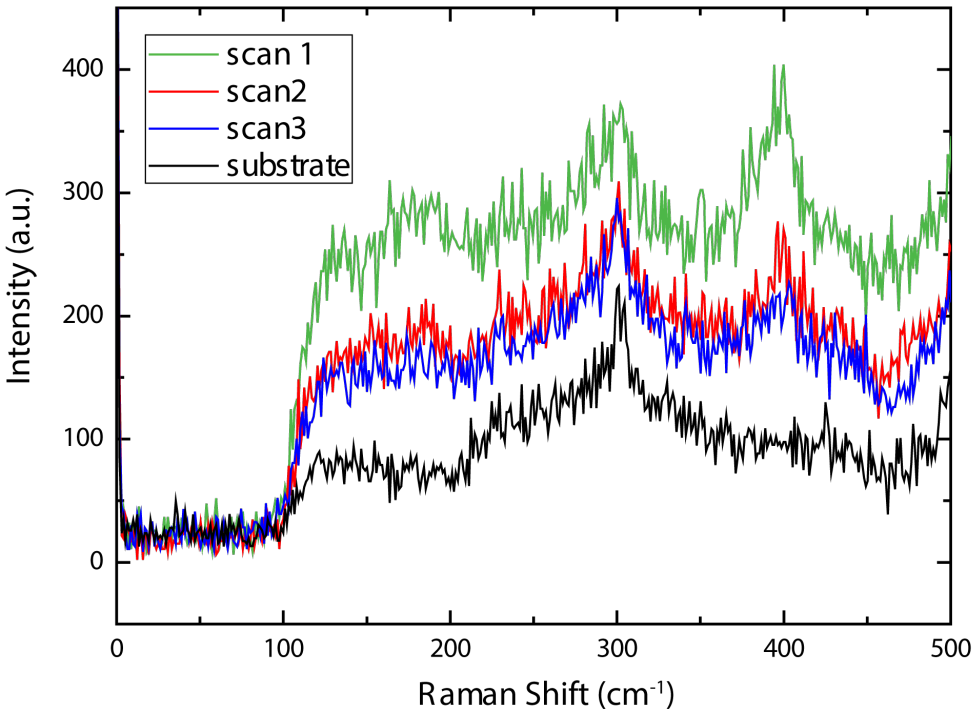

Figure 6.4: A TaS_2 flake scanned 3 times to etch it.

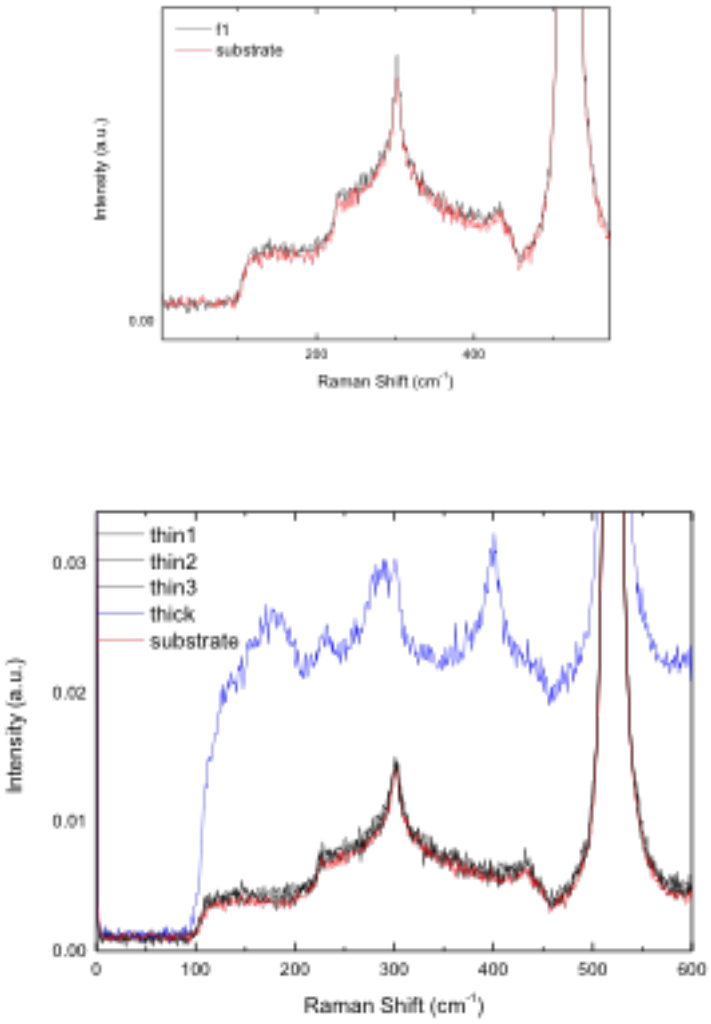

Figure 6.5: Flakes after area etching compared to the substrate background.

Chapter 7

Few layer Raman study of 2H-$NbSe_2$

$NbSe_2$ has shown interesting properties. For example. Recent studies have focussed on few layer $NbSe_2$ [36] however monolayer $NbSe_2$ has been less investigated due to the difficulty to isolate it. The aim of this chapter is to investigate the Raman properties of few layer flakes and see the effect of etching them with a laser to reduce their thickness in a controlled way.

7.1 $NbSe_2$ Raman response for different thickness

$NbSe_2$ flakes with different number of layers were produced by mechanical exfoliation of bulk crystals as described in section 3.1 of chapter 3. Contrast measurements were used to assess the thickness of the flakes, as discussed in chapter 3. In total 14 flakes of different thicknesses were investigated. Figure 7.1 shows the Raman spectra for some representative $NbSe_2$ flakes with different number of layers (f1-f4). Sample f4 was 3 layers thick, f3 was 2 layers thick and f1 was one layer thick. In addition the Raman spectra of the bulk material and of the substrate are also presented in this figure. The Raman signal gives 3 main peaks; one around 190 cm^{-1}, a second sharper peak at around 230 cm^{-1}, and a third at about 250 cm^{-1}. For all number of layers all the peaks reduce in intensity with decreasing number of layers, with the peak at 230cm^{-1} reducing faster than the peak at 250cm^{-1}. The highest intensity is the bulk, followed by the 3 layered $NbSe_2$. The 2 layered and monolayer $NbSe_2$ are very similar in intensity except for the ratio of the 230 and 250cm^{-1} peaks which is reversed.

On its second time scanned f4 shows little change from the bulk material (f4 was scanned multiple times to see whether the material was being etched by the measurement). The 5th scan of f4 shows that it had been reduced to have a similar signal to that of the 2 layer f3 sample, with a marked reduction in the second peak's intensity.

Each scan was very short at 1% power for 10 seconds because the material etched very easily and even at this power the material was thinned by successive scans.

7.2 Raman response to etching of flakes

Following from the initial Raman scans, a more detailed study was conducted to explore the effect of etching on the $NbSe_2$ flakes. In figure 7.2, multiple scans of one

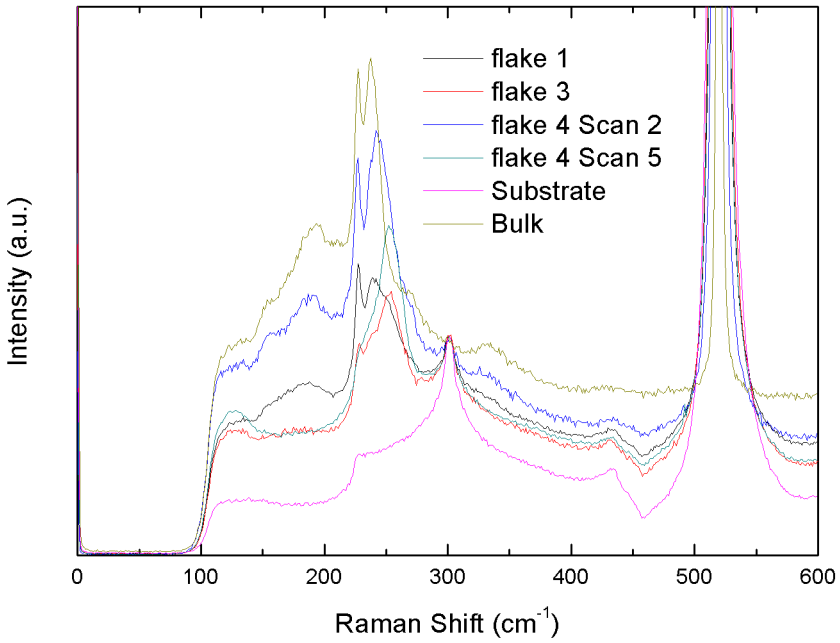

Figure 7.1: Raman spectrum of flakes of varying thickness of $NbSe_2$ including bulk.

point on a flake about 10 layers thick reduces the intensity of the 3 main peaks in the Raman spectrum. The intensity of the second peak reduces slightly more quickly in comparison to the third. After 5 scans the peak intensities are reduced to just a single peak, around 250 cm^{-1}. The single peak does not appear to change after this point, suggesting the material has been reduced to a monolayer and cannot be reduced further.

This is also reflected in the previous figure 7.1, where the 3 layer f4 sample is scanned multiple times and from the second scan to the 5th scan it is reduced in intensity similar to that of a 2 layer or monolayer. It also has a marked reduction in the second peak's intensity which seems to match the 2 layer sample.

For a thin flake of a single layer the starting Raman signal only contained one peak around 250 cm^{-1} which changed the intensity a bit when scanned but did not disappear after multiple scans.

This study shows that it is possible to etch down the number of layers of few layer $NbSe_2$ to a single layer in a controlled way. The etching does require a short exposure time and low laser intensity so it may not be possible to extend this to etch areas easily because of the extended periods and intensities of the laser on the surface.

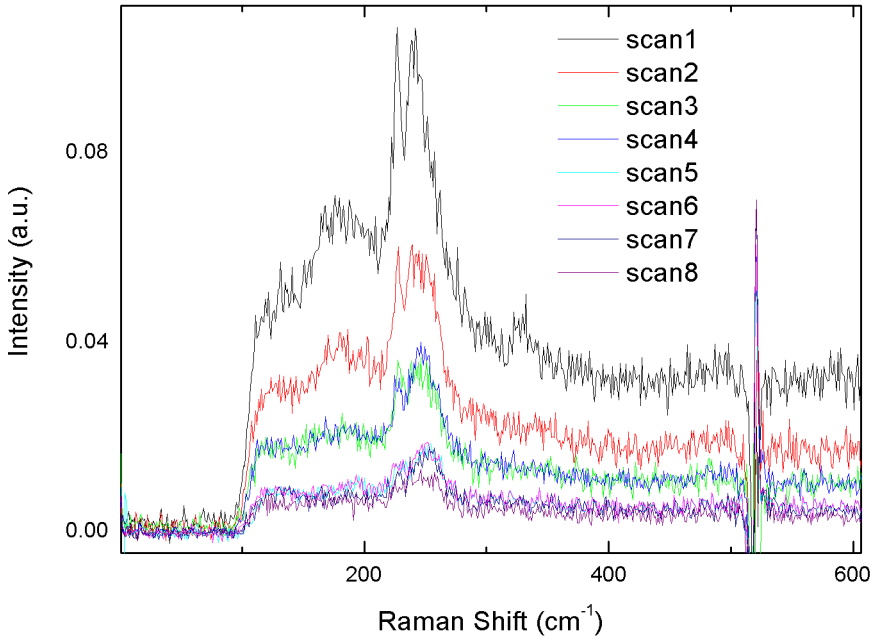

Figure 7.2: A $NbSe_2$ flake scanned 8 times to etch it (normalised with the background substrate removed).

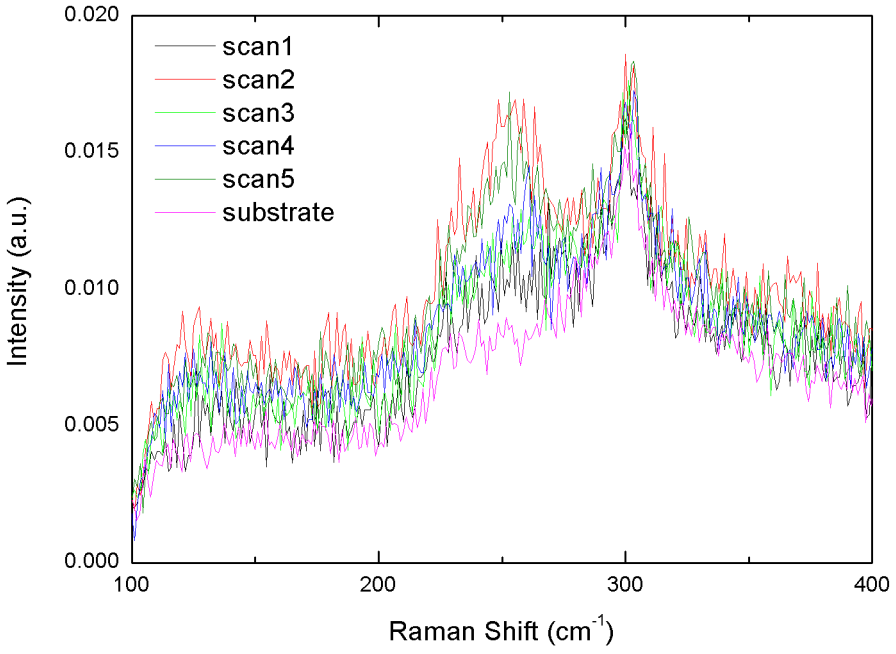

Figure 7.3: A thin $NbSe_2$ flake scanned 5 times to etch it.

Chapter 8

Conclusions

This thesis focussed on the functionalization of few layer graphene with the intercalent $FeCl_3$ and whether the intercalent and its effects remained intact after etching into shapes that were on the order of a few hundred nanometres wide. The Raman spectra of the graphene G peak and 2D peak were altered when the intercalent was first added to large samples, and remained modified in the same way after patterning into 200nm and 300nm wide ribbons. The electrical measurements taken after intercalation and patterning also show an increase in conductivity compared to pristine unintercalated graphene samples. Both these results seem to indicate that the intercalent has stayed within the graphene layers and continue to influence the Raman and electrical properties even when exposed to electron beam patterning techniques which reduces the sample width.

The effect of graphene as a substrate for plasmons showed that there was a change to the attenuation corresponding to the number of layers of the few layered graphene used. This change did not appear to influence the refractive index, but only the reflected optical field. The resonance peak was affected by each successive layer added, without affecting the refractive index, due to the thinness of the graphene layers. This linear relationship between the resonance peak and the number of layers was present in both intercalated and pristine graphene.

The Raman studies on 1T-TaS_2 and $NbSe_2$ showed promise that the Raman laser spot could be used to reduce the number of layers of the few layer samples of both materials in a controlled manor, but these Raman studies are only preliminary and could be considered an interesting possibility for future study of further experiments and conditions.

Bibliography

[1] Ruitao Lv, Joshua A. Robinson, Raymond E. Schaak, Du Sun, Yifan Sun, Thomas E. Mallouk, and Mauricio Terrones. Transition metal dichalcogenides and beyond: Synthesis, properties, and applications of single- and few-layer nanosheets. *Accounts of Chemical Research*, 48(1):56–64, 2015.

[2] A. H. Castro Neto, F. Guinea, N. M. R. Peres, K. S. Novoselov, and A. K. Geim. The electronic properties of graphene. *Rev. Mod. Phys.*, 81(1):109–162, January 2009.

[3] A. K. Geim. Graphene: Status and prospects. *Science*, 324(5934):1530–1534, 2009.

[4] Mikito Koshino. Interlayer screening effect in graphene multilayers with aba and abc stacking. *Phys. Rev. B*, 81(12):125304, March 2010.

[5] Mikito Koshino and Tsuneya Ando. Orbital diamagnetism in multilayer graphenes: Systematic study with the effective mass approximation. *Phys. Rev. B*, 76(8):085425, August 2007.

[6] R. R. Nair, P. Blake, A. N. Grigorenko, K. S. Novoselov, T. J. Booth, T. Stauber, N. M. R. Peres, and A. K. Geim. Fine structure constant defines visual transparency of graphene. *Science*, 320:1308, 2008.

[7] A. C. Ferrari, J. C. Meyer, V. Scardaci, C. Casiraghi, M. Lazzeri, F. Mauri, S. Piscanec, D. Jiang, K. S. Novoselov, S. Roth, and A. K. Geim. Raman spectrum of graphene and graphene layers. *Phys. Rev. Lett.*, 97(18):187401, October 2006.

[8] L.M. Malard, M.A. Pimenta, G. Dresselhaus, and M.S. Dresselhaus. Raman spectroscopy in graphene. *Physics Reports*, 473(5-6):51–87, 2009.

[9] S. H. Jhang, M. F. Craciun, S. Schmidmeier, S. Tokumitsu, S. Russo, M. Yamamoto, Y. Skourski, J. Wosnitza, S. Tarucha, J. Eroms, and C. Strunk. Stacking-order dependent transport properties of trilayer graphene. *Phys. Rev. B*, 84(16):161408, October 2011.

[10] Yee Kan Koh, Myung-Ho Bae, David G. Cahill, and Eric Pop. Reliably counting atomic planes of few-layer graphene (n >4). *ACS Nano*, 5(1):269–274, 2011.

[11] Da Zhan, Li Sun, Zhen Hua Ni, Lei Liu, Xiao Feng Fan, Yingying Wang, Ting Yu, Yeng Ming Lam, Wei Huang, and Ze Xiang Shen. $FeCl_3$-based few-layer graphene intercalation compounds: Single linear dispersion electronic band structure and strong charge transfer doping. *Adv. Funct. Mater.*, 20(20):3504–3509, October 2010.

[12] M. F. Craciun, S. Russo, M. Yamamoto, J. B. Oostinga, A. F. Morpurgo, and S. Tarucha. Trilayer graphene is a semimetal with a gate-tuneable band overlap (supplementary material). *Nat. Nanotech*, 4:383–388, 2009.

[13] Matthias Koch, Francisco Ample, Christian Joachim, and Leonhard Grill. Voltage-dependent conductance of a single graphene nanoribbon. *Nature Nanotechnology*, 7(11):713–717, November 2012.

[14] Peng Zheng, Sarah E. Bryan, Yinxiao Yang, Raghu Murali, Azad Naeemi, and James D. Meindl. Hydrogenation of graphene nanoribbon edges:improvement in carrier transport. *IEEE Electron Device Letters*, 34(5):707–709, May 2013.

[15] Jens Baringhaus, Ming Ruan, Frederik Edler, Antonio Tejeda, Muriel Sicot, Taleb-IbrahimiAmina, An-Ping Li, Zhigang Jiang, Edward H. Conrad, Claire Berger, Christoph Tegenkamp, and Walt A. de Heer. Exceptional ballistic transport in epitaxial graphene nanoribbons. *Nature*, 506(7488):349–354, 02 2014.

[16] Ankur Gupta, Tamilselvan Sakthivel, and Sudipta Seal. Recent development in 2d materials beyond graphene. *Progress in Materials Science*, 73:44–126, August 2015.

[17] K. S. Novoselov, A. K. Geim, S. V. Morozov, D. Jiang, Y. Zhang, S. V. Dubonos, I. V. Grigorieva, and A. A. Firsov. Electric field effect in atomically thin carbon films. *Science*, 306(5696):666–669, October 2004.

[18] A. K. Geim and K. S. Novoselov. The rise of graphene. *Nature Materials*, 6:183–191, 2007.

[19] H. Pinto, R. Jones, J. P. Goss, and P. R. Briddon. Mechanisms of doping graphene. *physica status solidi (a)*, 207(9):2131–2136, 2010.

[20] Hai Li, Gang Lu, Yanlong Wang, Zongyou Yin, Chunxiao Cong, Qiyuan He, Lu Wang, Feng Ding, Ting Yu, and Hua Zhang. Mechanical exfoliation and characterization of single- and few-layer nanosheets of WSe2, TaS2, and TaSe2. *Small*, 9(11):1613–6829, 2013.

[21] Frank Schwierz. Graphene transistors. *Nat Nano*, 5(7):487–496, 07 2010.

[22] M. F. Craciun, S. Russo, M. Yamamoto, and S. Tarucha. Tuneable electronic properties in graphene. *Nano Today*, 6:42–60, 2011.

[23] M F Craciun, I Khrapach, M D Barnes, and S Russo. Properties and applications of chemically functionalized graphene. *Journal of Physics: Condensed Matter*, 25(42):423201, 2013.

[24] Weijie Zhao, Ping Heng Tan, Jian Liu, and Andrea C. Ferrari. Intercalation of few-layer graphite flakes with FeCl3: Raman determination of fermi level, layer by layer decoupling, and stability. *Journal of the American Chemical Society*, 133(15):5941–5946, 2011.

[25] P. Blake, E. W. Hill, A. H. Castro Neto, K. S. Novoselov, D. Jiang, R. Yang, T. J. Booth, and A. K. Geim. Making graphene visible. *Applied Physics Letters*, 91(6), 2007.

[26] Sukang Bae, Hyeongkeun Kim, Youngbin Lee, Xiangfan Xu, Jae-Sung Park, Yi Zheng, Jayakumar Balakrishnan, Tian Lei, Hye Ri Kim, Young Il Song, Young-Jin Kim, Kwang S. Kim, Barbaros Ozyilmaz, Jong-Hyun Ahn, Byung Hee Hong, and Sumio Iijima. Roll-to-roll production of 30-inch graphene films for transparent electrodes. *Nat Nano*, 5(8):574–578, August 2010.

[27] Claire Berger, Zhimin Song, Tianbo Li, Xuebin Li, Asmerom Y. Ogbazghi, Rui Feng, Zhenting Dai, Alexei N. Marchenkov, Edward H. Conrad, Phillip N. First, and Walt A. de Heer. Ultrathin epitaxial graphite: 2d electron gas properties and a route toward graphene-based nanoelectronics. *J Phys Chem B*, 108(52):19912–19916, December 2004.

[28] Kyoko Nakada, Mitsutaka Fujita, Gene Dresselhaus, and Mildred Dresselhaus. Edge state in graphene ribbons: Nanometer size effect and edge shape dependance. *Phys. Rev. B*, 54(24):17954–17961, December 1996.

[29] C. Stampfer, J. Güttinger, S. Hellmütter, F. Molitor, K. Ensslin, and T. Ihn. Energy gaps in etched graphene nanoribbons. *Phys. Rev. Lett.*, 102(5):056403, Febuary 2009.

[30] Jeroen B. Oostinaga, Benjamin Sacépé, Monica F. Craciun, and Alberto F. Morpurgo. Magnetotransport through graphene nanoribbons. *Phys. Rev. B*, 81(19):193408, May 2010.

[31] Wei Lu, Gedeng Ruan, Bostjan Genorio, Yu Zhu, Barbara Novosel, Zhiwei Peng, and James M. Tour. Functionalized graphene nanoribbons via anionic polymerization initiated by alkali metal-intercalated carbon nanotubes. *ACS Nano*, 7(3):2669–2675, Febuary 2013.

[32] Wei Cao, Tao Huang, Xiao-Hong Nancy Xu, and Hani E. Elsayed-Ali. Localized surface plasmon resonance of single silver nanoparticles studied by dark-field optical microscopy and spectroscopy. *Journal of Applied Physics*, 109(3):034310, 2018/03/21 2011.

[33] W. Andrew Murray, Baptiste Auguié, and William L. Barnes. Sensitivity of localized surface plasmon resonances to bulk and local changes in the optical environment. *The Journal of Physical Chemistry C*, 113(13):5120–5125, 04 2009.

[34] W. Andrew Murray, James. R. Suckling, and William L. Barnes. Overlayers on silver nanotriangles: Field confinement and spectral position of localized surface plasmon resonances. *Nano Letters*, 6(8):1772–1777, 08 2006.

[35] Parviz Hajiyev, Chunxiao Cong, Caiyu Qiu, and Ting Yu. Contrast and raman spectroscopy study of single- and few-layered charge density wave material: 2h-tase2. *Scientific Reports*, 3:2593 EP –, 09 2013.

[36] Xiaoxiang Xi, Liang Zhao, Zefang Wang, Helmuth Berger, László Forró, Jie Shan, and Kin Fai Mak. Strongly enhanced charge-density-wave order in monolayer nbse2. *Nature Nanotechnology*, 10:765 EP –, 07 2015.

Acknowledgements

I wish to thank firstly my family, especially my parents and loving wife Nhu, who have been with me and supported me throughout this whole process. I would also like to thank my patient and intelligent supervisor Monica Craciun, her partner Saverio Russo as well as my fellow PhD students, especially those who I collaborated with, Tom Bointon, Dima Polyushkin and Ivan Khrapach. Their help has been invaluable in this long process.